An N-terminal motif in NLR immune receptors is functionally conserved across distantly related plant species

Hiroaki Adachi[1], Mauricio Contreras[1], Adeline Harant[1], Chih-hang Wu[1], Lida Derevnina[1], Toshiyuki Sakai[1], Cian Duggan[2], Eleonora Moratto[2], Tolga O Bozkurt[2], Abbas Maqbool[1], Joe Win[1], Sophien Kamoun[1*]

[1]The Sainsbury Laboratory, University of East Anglia, Norwich Research Park, Norwich NR4 7UH, United Kingdom.
[2]Imperial College London, Department of Life Sciences, London SW7 2AZ, United Kingdom.
*Corresponding author

The molecular codes underpinning the functions of plant NLR immune receptors are poorly understood. We used *in vitro* Mu transposition to generate a random truncation library and identify the minimal functional region of NLRs. We applied this method to NRC4—a helper NLR that functions with multiple sensor NLRs within a Solanaceae receptor network. This revealed that the NRC4 N-terminal 29 amino acids are sufficient to induce hypersensitive cell death. This region is defined by the consensus MADAxVSFxVxKLxxLLxxEx (MADA motif) that is conserved at the N-termini of NRC family proteins and ~20% of coiled-coil (CC)-type plant NLRs. The MADA motif matches the N-terminal α1 helix of Arabidopsis NLR protein ZAR1, which undergoes a conformational switch during resistosome activation. Immunoassays revealed that the MADA motif is functionally conserved across NLRs from distantly related plant species. NRC-dependent sensor NLRs lack MADA sequences indicating that this motif has degenerated in sensor NLRs over evolutionary time.

Plants have evolved intracellular immune receptors to detect host-translocated pathogen virulence proteins, known as effectors (Dodds and Rathjen, 2010; Jones et al., 2016; Kourelis and van der Hoorn, 2018). These receptors, encoded by disease resistance (*R*) genes, are primarily nucleotide-binding, leucine-rich repeat proteins (NLRs). NLR-triggered immunity (also known as effector-triggered immunity) includes the hypersensitive response (HR), a type of programmed cell death associated with disease resistance. NLRs are widespread across eukaryotes and have been described in animals and fungi in addition to plants (Jones et al., 2016). In contrast to other taxa, plants express very large and diverse repertoires of NLRs, with anywhere from about 50 to 1000 genes encoded per genome (Shao et al., 2016; Steuernagel et al., 2018). Genome-wide analyses have defined repertoires of NLRs (NLRome) across plant species (Shao et al., 2016). An emerging paradigm is that plant NLRs form receptor networks with varying degrees of complexity (Wu et al., 2018). NLRs have probably evolved from multifunctional singleton receptors—which combine pathogen detection (sensor activity) and immune signalling (helper or executor activity) into a single protein—to functionally specialized interconnected receptor pairs and networks (Adachi et al., 2019a). However, our knowledge of the functional connections and biochemical

mechanisms underpinning plant NLR networks remains limited. In addition, although dozens of NLR proteins have been subject to functional studies since their discovery in the 1990s, this body of knowledge has not been interpreted through an evolutionary biology framework that combines molecular mechanisms with phylogenetics.

NLRs are multidomain proteins of the ancient group of Signal Transduction ATPases (STAND) proteins that share a nucleotide-binding (NB) domain. In addition to the NB and LRR domains, most plant NLRs have characteristic N-terminal domains that define three subgroups: coiled-coil (CC), CC_R or RPW8-like (RPW8) and toll and interleukin-1 receptor (TIR) (Shao et al., 2016). In metazoans, NLRs confer immunity to diverse pathogens through a wheel-like oligomerization process resulting in multiprotein platforms that recruit downstream elements, such as caspases (Qi et al., 2010; Zhou et al., 2015; Hu et al., 2015; Zhang et al., 2015; Tenthorey et al., 2017). Plant NLRs have long been thought to oligomerize through their N-terminal domains when they're activated (Bentham et al., 2017). However, the precise molecular mechanisms that underpin NLR activation and subsequent execution of HR cell death have remained largely unknown until very recently. In two remarkable papers, Wang et al. (2019a; 2019b) have significantly advanced our understanding of both the structural and biochemical basis of CC-NLR activation in plants. They reconstituted the inactive and active complexes of the Arabidopsis CC-NLR ZAR1 (HOPZ-ACTIVATED RESISTANCE1) with its partner receptor-like cytoplasmic kinases (RLCKs) (Wang et al., 2019a; 2019b). Cryo-electron microscopy (cryo-EM) structures revealed that activated ZAR1 forms a resistosome—a wheel-like pentamer that undergoes a conformational switch to expose a funnel-shaped structure formed by the N-terminal α helices (α1) of the CC domains (Wang et al., 2019a; 2019b). They propose an engaging model in which the exposed α1 helices of the ZAR1 resistosome mediate cell death by translocating into the plasma membrane and perturbing membrane integrity similar to pore-forming toxins (Wang et al., 2019b). However, whether the ZAR1 model extends to other CC-NLRs is unknown. One important unanswered question is the extent to which the α1 helix "death switch" occurs in other CC-NLRs (Adachi et al., 2019b).

Although ZAR1 is classified as a singleton NLR that detects pathogen effectors without associating with other NLRs, many plant NLRs are interconnected in NLR pairs or networks (Wu et al., 2018; Adachi et al., 2019a). Paired and networked NLRs consist of sensor NLRs that detect pathogen effectors and helper NLRs that translate this effector recognition into HR cell death and immunity. In the Solanaceae, a major phylogenetic clade of CC-NLRs forms a complex immunoreceptor network in which multiple helper NLRs, known as NLR-REQUIRED FOR CELL DEATH (NRC), are required by a large number of sensor NLRs, encoded by *R* gene loci, to confer resistance against diverse pathogens, such as viruses, bacteria, oomycetes, nematodes and insects (Wu et al., 2017). These proteins form the NRC superclade, a well-supported phylogenetic cluster divided into the NRC helper clade (NRC-helpers or NRC-H) and a larger clade that includes all known NRC-dependent sensor NLRs (NRC-sensors or NRC-S) (Wu et al., 2017). The NRC superclade has expanded over 100 million years ago (Mya) from an NLR pair that diversified to up to one-half of the NLRs of asterid plants (Wu et al., 2017). How this diversification has impacted the biochemical activities of the NRC-S compared to their NRC-H mates is poorly understood. For example, it's unclear how the ZAR1 conceptual framework applies to more complex NLR configurations such as the NRC network (Adachi et al., 2019b).

This paper originates from use of the *in vitro* Mu transposition system to generate a random truncation library and identify the minimal region required for CC-NLR-mediated cell death. We applied this method to NRC4—a CC-NLR helper of the NRC family that is genetically required by a multitude of NRC-S, such as the potato late blight resistance protein Rpi-blb2, to cause HR cell death and confer disease resistance (Wu et al., 2017). This screen revealed that the N-terminal 29 amino acids of NRC4 are sufficient to induce cell death. Remarkably, this region is about 50% identical to the N-terminal ZAR1 α1 helix, which undergoes the conformational "death switch" associated with the activation of the ZAR1 resistosome (Wang et al., 2019b). Computational analyses revealed that this region is defined by a motif, following the consensus MADAxVSFxVxKLxxLLxxEx, which we coined the "MADA motif". This sequence is conserved not only in NRC4 and ZAR1 but also in ~20% of all CC-NLRs of dicot and monocot species. Motif swapping experiments revealed that the MADA motif is functionally conserved between NRC4 and ZAR1, as well as between NLRs from distantly related plant species. Interestingly, NRC-S lack N-terminal MADA sequences, which may have become non-functional over evolutionary time. We conclude that the evolutionarily constrained MADA motif is critical for the cell death inducing activity of CC domains from a significant fraction of plant NLR proteins, and that the "death switch" mechanism defined for the ZAR1 resistosome is probably widely conserved across singleton and helper CC-NLRs.

Results

Mu mutagenesis of NRC4 reveals a short 29 amino acid N-terminal region that is sufficient for induction of HR cell death

The N-terminal CC domain of a subset of CC-NLR proteins can mediate self-association and trigger HR cell death when expressed on its own (Bentham et al., 2018). However, to date truncation experiments have been conducted based on educated guesses of domain boundaries (Maekawa et al., 2011; Casey et al., 2016; Cesari et al., 2016; Wróblewski et al., 2018). Moreover, one amino acid difference in the length of the assayed truncation can affect cell death inducing activity (Casey et al., 2016). Therefore, we designed an unbiased truncation approach using bacteriophage Mu *in vitro* transposition system to randomly generate a C-terminal deletion library of the helper NLR NRC4. By using a custom-designed artificial transposon (Mu-STOP transposon) that carries staggered translation stop signals at Mu R-end (Poussu et al., 2005), we targeted the full-length coding sequence of the NRC4 autoactive mutant, NRC4^{D478V}, (referred to from here on as NRC4^{DV}). We generated a total of 65 truncated NRC4^{DV}::Mu-STOP variants and expressed these mutants in *Nicotiana benthamiana* leaves using agroinfiltration (Figure 1A). Remarkably, only a single truncate carrying the N-terminal 29 amino acids triggered visible cell death in *N. benthamiana* leaves (Figure 1B, Figure 1—figure supplement 1). To validate this phenotype, we expressed NRC4 N-terminal 29 amino acids (NRC4$_{1\text{-}29}$) fused with the yellow fluorescent protein (YFP) at the C-terminus in *N. benthamiana* leaves (Figure 2A). NRC4$_{1\text{-}29}$-YFP triggered a visible cell death response, although the cell death intensity was weaker than that of the full-length NRC4^{DV}-YFP (Figure 2B-E).

To determine whether NRC4$_{1\text{-}29}$-YFP requires the endogenous *N. benthamiana* NRC4 to trigger cell death, we expressed this fusion protein in two independent mutant *nrc4a/b*

plants that carry CRISPR/Cas9-induced mutations in the two NRC4 genes *NRC4a* and *NRC4b* (Figure 2—figure supplement 1, see methods). In these plants, $NRC4_{1\text{-}29}$-YFP still induced cell death indicating that the activity of the N-terminal 29 amino acids of NRC4 is independent of a full-length NRC4 protein (Figure 2C-D and F-G).

The CC domains of ZAR1 and maize Rp1 (RESISTANCE to PUCCINIA 1) are autoactive when expressed as a fusion protein with a fluorescent protein tag (Wang et al., 2015; Baudin et al., 2017). Given that YFP and related fluorescent proteins self-oligomerize (Kim et al., 2015), we hypothesized that such fluorescent proteins promote self-assembly of the N-terminal 29 amino acids of NRC4 resulting in hypersensitive cell death. To test this hypothesis, we modified YFP with the alanine 206 (A206) to lysine (K) mutation that reduces homo-affinity (Figure 2—figure supplement 2A) (Zacharias et al., 2002). The YFP^{A206K} mutation compromised the cell death intensity of $NRC4_{1\text{-}29}$-YFP but not that of full-length $NRC4^{DV}$ (Figure 2—figure supplement 2B-E). This result indicates that YFP-mediated self-assembly is a key step in the capacity of $NRC4_{1\text{-}29}$-YFP to trigger hypersensitive cell death.

NRC4 carries N-terminal sequences that are conserved across distantly related CC-NLRs

Our finding that the N-terminal 29 amino acids of NRC4 are sufficient to trigger cell death prompted us to investigate the occurrence of this sequence across the plant NLRome. We first compiled a sequence database containing 988 putative CC-NLRs and CC_R-NLRs (referred to from here on as CC-NLR database, Figure 3A, Figure 3—figure supplement 1) from 6 representative plant species (Arabidopsis, sugar beet, tomato, *N. benthamiana*, rice and barley) amended with 23 functionally characterized NLRs. Next, we extracted their sequences prior to the NB-ARC domain (Figure 3A). These sequences were too diverse and aligned poorly to each other to enable global phylogenetic analyses. Therefore, to classify the extracted N-terminal sequences based on sequence similarity, we clustered them into protein families using Markov cluster (MCL) algorithm Tribe-MCL (Enright et al., 2002) (Figure 3A). The 988 proteins clustered into 59 families of at least two sequences (tribes) and 43 singletons (Figure 3B). The largest tribe, Tribe 1, consists of 219 monocot NLRs, including MLA10, Sr33, Sr50, the paired Pik and Pia (RGA4 and RGA5) NLRs, and 7 dicot NLRs notably RPM1 (Figure 3B). Tribe 2, the second largest tribe with 102 proteins, consists primarily of dicot proteins (93 out of 102) but still includes 9 monocot NLRs. Interestingly, Tribe 2 grouped NRC-H proteins, including NRC4, with well-known CC-NLRs, such as ZAR1, RPP13, R2 and Rpi-vnt1.3 indicating that these proteins share similarities in their CC domains (Figure 3B).

We performed phylogenetic analyses of NLR proteins using the NB-ARC domain because it is the only conserved domain that produces reasonably good global alignments and can inform evolutionary relationships between all members of this family (Figure 3—figure supplement 2). We mapped individual NLR proteins grouped in Tribe-MCL N-terminal tribes onto a phylogenetic tree based on the NB-ARC domain (Figure 3C). These analyses revealed that the clustering of NLRs into the N-terminal tribes does not always match the NB-ARC phylogenetic clades (Figure 3C). In particular, NLRs in Tribe 1 and Tribe 2 often mapped to distinct well-supported clades scattered throughout the NB-ARC phylogenetic tree. We conclude that there are N-terminal domain sequences that have remained conserved over evolutionary time across distantly related CC-NLRs.

NRC4 and ZAR1 share the N-terminal MADA motif

Next, we investigated whether N-terminal domains of CC-NLRs carry specific sequence motifs. We used MEME (Multiple EM for Motif Elicitation) (Bailey and Elkan, 1994) to identify conserved patterns in each of the N-terminal domain tribes. MEME revealed several conserved sequence patterns in each of the four largest tribes (Figure 4—figure supplement 1). The previously reported sequence pattern, EDVID motif (Rairdan et al., 2008), was as expected predicted in ~87 to 96% in the four largest tribes (Figure 4—figure supplement 1). Within Tribe 2, a motif that is conserved at the N terminus of 87 of 102 proteins overlapped with the N-terminal 29 amino acids of NRC4 we identified as sufficient to cause cell death (Figure 4—figure supplement 1). Remarkably, the conserved sequence pattern of this very N-terminal motif matched the ZAR1 α1 helix that undergoes a conformational switch during activation of the ZAR1 resistosome (Wang et al., 2019b) (Figure 4A-B). In fact, 8 of the first 17 amino acids of ZAR1 are invariant in NRC4, and the majority of the amino acid polymorphisms between ZAR1 and NRC4 in the α1 helix region are conservative (Figure 4A). We conclude that NRC4, ZAR1 and numerous other CC-NLRs share a conserved N-terminal motif. We coined this sequence "MADA motif" based on the deduced 21 amino acid consensus sequence MADAxVSFxVxKLxxLLxxEx (Figure 4A, Figure 4—figure supplement 2).

The MADA motif is primarily found in NLR proteins

We built a Hidden Markov Model (HMM) from a sequence alignment of the MADA motif of 87 NLR proteins from Tribe 2. To determine whether the MADA motif is primarily found among proteins annotated as NLRs, we used the HMMER software (Eddy, 1998) to query the Arabidopsis and tomato proteomes using the MADA motif HMM. HMMER searches revealed that the MADA motif is mainly found in NLR proteins compared with non-NLR proteins (Figure 4C). An HMM score cut-off of 10.0 clearly distinguishes NLR proteins from others with 97.1% (34 out of 35) tomato proteins and 97.7% (42 out of 43) Arabidopsis proteins scoring over 10.0 being annotated as NLRs (Figure 4C). We conclude that the MADA motif is a sequence signature of a subset of NLR proteins and that a HMMER cut-off score of 10.0 is most optimal for high confidence searches of MADA containing CC-NLR proteins (MADA-CC-NLRs).

MADA-like sequences occur in the N-termini of about 20% of dicot and monocot CC-NLRs

To what extent does the MADA motif occur in plant NLRomes? We re-screened the CC-NLR database using HMMER and identified 103 hits (10.4%) over the cut-off score of 10.0 (Figure 5A-B, Figure 5—figure supplement 1A). We also noted that another 129 NLRs were positive but with a score lower than 10.0, and we tentatively termed these hits as MADA-like CC-NLRs (MADAL-CC-NLRs) (Figure 5B, Figure 5—figure supplement 1A). Most of the MADA hits are from dicot plant species whereas MADAL-CC-NLRs are primarily from monocots possibly reflecting a bias in our HMM profile which was built from the dicot enriched Tribe 2 (Figure 5C, Figure 5—figure supplement 1B). Indeed, the majority of MADA hits (85 out of 103) were from Tribe 2, which includes NRC4 and ZAR1, but some MADA hits were also from other Tribes, notably the rice helper NLR Pik-2 from Tribe 1 (HMM score = 10.4) (Figure 5C, Figure 5—figure supplement 1C). MADAL-CC-NLRs are mainly from Tribe 1 and Tribe 4 and

include the monocot proteins MLA10 and Sr33, as well as Arabidopsis RPM1 (Figure 5C, Figure 5—figure supplement 1C).

Given that the MADA sequence is at the very N-terminus of ZAR1 and NRC4, and that the N-terminal position of the ZAR1 α1 helix is critical for its function based on the model of Wang et al. (2019b), we checked the positional distribution of predicted MADA and MADAL motifs (Figure 5D). The majority of the predicted MADA and MADAL motifs (199 out of 232, 85.8%) occurred at the very beginning of the NLR protein. However, 4 of 103 of the predicted MADA- and 29 of 129 MADAL-CC-NLRs have N-terminal extensions over 15 amino acids prior to the motifs (Figure 5D). For example, the MADA motif is located at position 54 to 72 amino acids in the potato NLR Rpi-vnt1.3. Whether these exceptions reflect misannotated gene models or genuinely distinct motif sequences remains to be determined.

In summary, our bioinformatic analyses revealed that 199 out 988 (20.1%) of the CC-NLRs of six representative dicot and monocot species contain a MADA or MADAL motif at their very N-termini. These MADA sequences have noticeable similarity to NRC4 and ZAR1.

NRC-dependent sensor NLRs (NRC-S) lack the MADA motif

NB-ARC domain phylogenetic trees revealed that the NRC superclade is divided into the NRC clade (NRC-H) and a larger clade that includes all known NRC-dependent sensor NLRs (NRC-S) (Wu et al., 2017). We noted that even though the NRC-H and NRC-S are sister clades based on NB-ARC phylogenetic analyses, they grouped into distinct N-terminal domain tribes in the Tribe-MCL analyses (Figure 6A). Whereas all NRC-H mapped to Tribe 2, NRC-S clustered into 8 different tribes (Figure 6A). This pattern indicates that unlike the NRCs, the N-terminal sequences of their NRC-S mates have diversified throughout evolutionary time.

Next, we mapped the occurrence of the MADA motif onto the NB-ARC phylogenetic tree and noted that the distribution of the MADA motif was uneven across the NRC superclade despite their phylogenetic relationship (Figure 6B). Whereas 20 out of 22 NRC-H have a predicted MADA motif at their N-termini, none of the 117 examined NRC-S were predicted as MADA-CC-NLR in the HMMER search (Figure 6B). In fact, 65 of 117 NRC-S, including the well know disease resistance proteins R1, Prf, Sw5b, Hero, Rpi-blb2 and Mi-1.2, have N-terminal extensions of ~600 amino acids, or more in the case of Prf, prior to their predicted CC domains (Figure 6B). These findings indicate the CC domains of NRCs and their NRC-S mates have experienced distinct evolutionary trajectories even though these NLR proteins share a common evolutionary origin.

MADA motif residues are required for NRC4 to trigger cell death

To experimentally validate our bioinformatic analyses, we performed site directed mutagenesis to determine the degree to which the MADA motif is required for the activity of NRC4. First, we followed up on the ZAR1 structure-function analyses of Wang et al. (2019b) who showed that three amino acids (phenylalanine 9 [F9], leucine 10 [L10] and leucine 14 [L14]) within the α1 helix/MADA motif are required for ZAR1-mediated cell death and bacterial resistance. We introduced a triple alanine substitution similar to the mutant of Wang et al. (2019b) into the autoactive NRC4^{DV} and found that this L9A/V10A/L14A

mutation significantly reduced, but did not abolish, NRC4^{DV} cell death inducing activity (Figure 7A-C). Given that the MADA motif, particularly the mutated L9, V10 and L14 sites, is primarily composed of hydrophobic residues, we reasoned that substitutions with the negatively charged glutamic acid (E) would be more disruptive than hydrophobic alanine. Therefore, we substituted L9, V10 and L14 with glutamic acid, and observed that the L9E/V10E/L14E mutation resulted in a more severe disruption of the cell death activity of NRC4^{DV} compared to the triple alanine mutant (Figure 7A-C). Both of the NRC4^{DV} triple alanine and glutamic acid mutant proteins accumulated to similar levels as NRC4^{DV} when expressed in *N. benthamiana* leaves indicating that the observed loss-of-function phenotypes were not due to protein destabilization (Figure 7D).

We further introduced the triple alanine mutation to NRC4$_{1-29}$-YFP and ZAR1$_{1-144}$-YFP (Figure 7—figure supplement 1A). ZAR1$_{1-144}$ matches the ZAR1 CC domain and is known to trigger cell death when expressed fused to a YFP tag (Baudin et al., 2017). The triple alanine mutation abolished the cell death triggered by both NRC4$_{1-29}$-YFP and ZAR1$_{1-144}$-YFP, supporting the view that MADA motifs are essential for the capacity of the N-termini of NRC4 and ZAR1 to cause cell death (Figure 7—figure supplement 1B-D).

Next, we performed single alanine and glutamic acid mutant scans to reveal which other residues in the MADA motif are required for NRC4-mediated cell death. None of the tested single alanine-substituted mutants affected the cell death response of NRC4^{DV} (Figure 8—figure supplement 1). In contrast, single glutamic acid mutations L9E, L13E and L17E essentially abolished the cell death activity of NRC4^{DV} without affecting the stability of the mutant proteins (Figure 8). Therefore, we determined that the L9, L13, and L17 residues in the MADA motif are critical for cell death induction by NRC4.

Finally, we mapped L9, L13 and L17 onto a homology model of the CC domain of NRC4 produced based on the ZAR1 resistosome structure of Wang et al. (2019b) (Figure 8—figure supplement 2). All three residues mapped to the outer surface of the funnel-shaped structure formed by the α1 helices similar to the previously identified residues in positions 9, 10 and 14. These results suggest that the outer surface of the funnel-shaped structure formed by N-terminal helices is critical not only for the function of ZAR1 but also for the activity of another MADA-CC-NLR.

NRC4$_{1-29}$-YFP forms MADA motif- and YFP-dependent puncta

The ZAR1 model postulates that the resistosome translocates into the plasma membrane through the α1 helix which matches the MADA motif (Wang et al., 2019b). To investigate the intracellular dynamics of the MADA motif, we analysed the subcellular distribution of NRC4$_{1-29}$-YFP in *N. benthamiana* leaves (Figure 9A). Interestingly, unlike free YFP which typically shows nucleocytoplasmic distribution, NRC4$_{1-29}$-YFP produced fluorescence signal in punctate structures throughout the cell in addition to relatively weak nucleocytoplasmic signal (Figure 9A). Furthermore, we merged both the z-stack and single plain images of the YFP proteins with the plasma membrane marker RFP-Rem1.3 (Bozkurt et al., 2014). Although the NRC4$_{1-29}$-YFP puncta did not completely overlap with RFP-Rem1.3 signal, we noticed some of the NRC4$_{1-29}$-YFP puncta associated with the plasma membrane (Figure 9A-B).

To further study the NRC4$_{1-29}$-YFP puncta, we examined puncta formation of the YFP A206K mutant, which shows reduced cell death by NRC4$_{1-29}$-YFP (Figure 2—figure supplement 2). In contrast to NRC4$_{1-29}$-YFP, NRC4$_{1-29}$-YFP^{A206K} rarely formed puncta (Figure 9A, C), suggesting that YFP self-assembly is required for NRC4$_{1-29}$-YFP puncta formation. Furthermore, introducing the L9E in NRC4$_{1-29}$-YFP greatly reduced puncta formation (Figure 9A, C). This finding directly connects puncta formation to the activity of full length NRC4 given that L9E also affects NRC4 cell death activity (Figure 8). Taken together, these results indicate that both an intact MADA motif and YFP oligomerization are required for the capacity of NRC4$_{1-29}$-YFP to form puncta as well as cause cell death in *N. benthamiana* leaves.

The α1 helix of Arabidopsis ZAR1 and the N-termini of other MADA-CC-NLRs can functionally replace the N-terminus of NRC4

Our observation that the ZAR1 α1 helix has sequence similarity to the N-terminus of NRC4 prompted us to determine whether this sequence is functionally conserved between these two proteins. To test this hypothesis, we swapped the first 17 amino acids of NRC4^{DV} with the equivalent region of ZAR1 (Figure 10A-B). The resulting ZAR1$_{1-17}$-NRC4 chimeric protein can still trigger cell death in *N. benthamiana* leaves indicating that the MADA/α1 helix sequence is functionally equivalent between these two NLR proteins (Figure 10C, Figure 10—figure supplement 1).

Next, we swapped the same 17 amino acids of NRC4 with the matching sequences of the MADA-CC-NLRs NRC2 from *N. benthamiana*, RPP8 and RPP13 from Arabidopsis, and Pik-2 and Os03g30910.1 from rice, all of which gave HMMER scores >10.0 and ranging from 30.8 to 10.4 (Figure 10A-B). All of the assayed chimeric NRC4^{DV} proteins retained the capacity to trigger cell death in *N. benthamiana* leaves (Figure 10C, Figure 10—figure supplement 1). We determined whether the N-termini of MADAL-CC-NLRs Arabidopsis RPM1 and barley MLA10, which yielded respective HMMER scores of 9.3 and 7.8, could also replace the first 17 amino acids of NRC4^{DV} (Figure 10A-B). Both NRC4^{DV} chimeras retained the capacity to trigger cell death indicating that these MADAL sequences are functionally analogous to the NRC4 N-terminus (Figure 10C, Figure 10—figure supplement 1). These results indicate that the MADA motif is functionally conserved even between distantly related NLRs from dicots and monocots.

We further swapped the 17 amino acids of NRC4^{DV} with N-terminal sequences from Arabidopsis LOV1 (AT1G10920), pepper Bs2 and potato Rx, all of which were not predicted to have a MADA sequences by HMMER searches (Figure 10A-B). LOV1 was among the 13.7% of Tribe 2 NLRs that were not predicted to have a MADA/MADAL motif. Bs2 and Rx are NRC-S NLRs that belong to different tribes—Tribe 11 and 25, respectively (Figure 6A). The N-terminal sequences of Bs2 and Rx are somewhat similar to MADA sequences but were negative in the HMMER analyses (Figure 10A). Interestingly, whereas the N-termini of Bs2 and LOV1 did not complement the cell death activity when swapped into NRC4^{DV}, Rx$_{1-17}$ could confer cell death activity when swapped into NRC4^{DV} (Figure 10C, Figure 10—figure supplement 1). This exception indicates that at least one of the N-terminal sequences that are not predicted as having the MADA motif may still functionally complement the N-terminus of NRC4.

ZAR1-NRC4 chimeric protein retains the capacity to confer Rpi-blb2-mediated resistance against the late blight pathogen *Phytophthora infestans*

We investigated whether the MADA motif of NRC4 is required for disease resistance against the oomycete pathogen *Phytophthora infestans*. One of the NRC4-dependent sensor NLRs is Rpi-blb2, an NRC-S protein from *Solanum bulbocastanum* that confers resistance to *P. infestans* carrying the matching effector AVRblb2 (van der Vossen et al., 2003; Oh et al., 2009). For this purpose, we set up a genetic complementation assay in which NRC4 is co-expressed with Rpi-blb2 in leaves of the *N. benthamiana nrc4a/b*_9.1.3 mutant prior to inoculation with the *P. infestans* strain 88069 (Wu et al., 2017), that carries AVRblb2 (Figure 11A). Unlike wild-type NRC4, the NRC4 L9A/V10A/L14A and L9E mutants failed to rescue the resistance to *P. infestans* in the *N. benthamiana nrc4a/b*_9.1.3 mutant, indicating that MADA motif mutations not only impair HR cell death as shown above but also affect disease resistance against an oomycete pathogen (Figure 11B). We conducted similar complementation assays with the $ZAR1_{1\text{-}17}$-NRC4 chimera in which the first 17 amino acids of NRC4 were swapped with the equivalent region of ZAR1, and found that $ZAR1_{1\text{-}17}$-NRC4 complemented the *nrc4a/b*_9.1.3 *N. benthamiana* mutant to a similar degree as wild-type NRC4 (Figure 11B). These experiments further confirm that the α1 helix/MADA motif of Arabidopsis ZAR1 is functionally equivalent to the N-terminus of NRC4, and that the chimeric $ZAR1_{1\text{-}17}$-NRC4 is not only able to trigger HR cell death but also retains its capacity to function with its NRC-S mate Rpi-blb2 and confer resistance to *P. infestans*.

Discussion

This study stems from a random truncation screen of the CC-NLR NRC4, which revealed that the very N-terminus of this protein is sufficient to carry out the HR cell death activity of the full-length protein. It turned out that this region is defined by a consensus sequence—the MADA motif—that occurs in about one fifth of plant CC-NLRs including Arabidopsis ZAR1. The MADA motif covers most of the functionally essential α1 helix of ZAR1 that undergoes a conformational switch during activation of the ZAR1 resistosome (Wang et al., 2019b). Our finding that the ZAR1 α1 helix/MADA motif can functionally replace its matching region in NRC4 indicates that the ZAR1 “death switch” mechanism may apply to NRCs and other MADA-CC-NLRs from dicot and monocot plant species.

We recently proposed that NLRs may have evolved from multifunctional singleton receptors to functionally specialized and diversified receptor pairs and networks (Adachi et al., 2019a). In this study, a striking finding from the computational analyses is that all NRC-S lack the MADA motif even though they are more closely related to NRC-H than to ZAR1 and other MADA-CC-NLRs in the NB-ARC phylogenetic tree (Figure 6). These observations led us to draw the evolutionary model of Figure 12. In this model, we propose that MADA-type sequences have emerged early in the evolution of CC-NLRs and have remained conserved from singletons to helpers in NLR pair and network throughout evolution. In sharp contrast, MADA sequences appear to have degenerated over time in sensor CC-NLRs as these proteins specialized in pathogen detection and lost the capacity to execute the immune response without their helper mates. Consistent with this view, NRC-H are known to be

more highly conserved than their NRC-S partners within the Solanaceae (Wu et al. 2017; Stam et al., 2019). Future analyses will determine whether MADA-CC-NLRs are generally more evolutionarily constrained than non-MADA containing NLRs.

In addition, about half of the NRC-S proteins have acquired N-terminal extensions (N-terminal domains) before their CC domain, which would preclude a free N-terminal α1 helix essential for a ZAR1 type "death switch" mechanism (Figure 6). In fact, the N-terminal domains of Prf and Sw5b function as baits that sense pathogen effectors, suggesting functional analogy to integrated effector detection motifs found in some NLRs, and are not known to be involved in executing the immune response (Saur et al., 2015; Li et al., 2019). Here, we hypothesize that the CC domains of these and other sensor NLRs have extensively diversified over evolutionary time and are losing the capacity to function as HR cell death executors. This could be a consequence of relaxed selection given that these proteins rely on their MADA-CC-NLR partners to execute the immune response as discussed above. Additional structure-function experiments will be needed to determine the extent to which this "use-it-or-lose-it" evolutionary model applies to the sensor sub-class of NLR immune receptors.

Understanding the precise nature of the N-terminal sequences that can functionally replace the α1 helix requires further investigation. In the MADA motif swap experiments, we found one exception to the correlation between MADA predictions and functional complementation of NRC4. The N-terminal sequence of the NRC-S NLR Rx, which was negative in the MADA HMMER searches, complemented the cell death activity of NRC4 MADA motif (Figure 10, Figure 10—figure supplement 1). Nonetheless, previously the NB domain of Rx was reported to be capable of triggering cell death (Rairdan et al., 2008), suggesting that the CC domain of Rx is dispensable for activation of HR. Therefore, in our "use-it-or-lose-it" model, the N-termini of some NRC-S may not have fully degenerated into non-functional sequences and may have residual ability to functionally complement MADA. In the future, it would be fascinating to determine resistosome configurations of NLR sensor and helper hetero-complexes. As discussed elsewhere (Adachi et al., 2019a; Jubic et al., 2019), one hypothesis is that sensor NLRs associate with the resistosome as functional equivalents of RLCKs in the ZAR1 resistosome. Another is that sensor NLRs form one of the wheel spokes in a hetero-oligomeric resistosome as in the mammalian NAIP/NLRC4 inflammasome (Tenthorey et al., 2017). It is possible that in this configuration, the N-terminus of a sensor NLR such as Rx remains evolutionarily constrained in terms of length and sequence composition. Future structural analyses of NLR sensor/helper heterocomplexes are needed to address these questions.

Already, our evolutionary model appears to be consistent with some paired NLR configurations in addition to the NRC-H/NRC-S network. One example is rice Pik-1 and Pik-2, which are a well-established NLR pair that detects the AVRPik effector of the rice blast fungus *M. oryzae* (Maqbool et al., 2015; Bialas et al., 2018). AVRPik binding to the integrated heavy metal associated (HMA) domain of Pik-1 results in HR cell death and blast fungus resistance only in the presence of its helper Pik-2 protein (Maqbool et al., 2015). In our computational analyses only Pik-2 was detected to carry an N-terminal MADA motif (Figure 5, HMM score = 10.4) even though the CC domains of both proteins grouped into Tribe 1 (Figure 3). The Pik-2 MADA motif could substitute for the N-terminus of NRC4 in our

cell death assays despite having 6 additional amino-acids at its N-terminus (Figure 10). These results are consistent with our Figure 11 model and imply that the helper NLR Pik-2 may execute HR cell death via its N-terminal MADA motif whereas its paired sensor NLR Pik-1 does not have the capacity to carry this activity on its own.

In addition to ZAR1, RPP8 is another Arabidopsis MADA-CC-NLR with high similarity to the N-terminus of NRC4 with 9 invariant amino acids out of 17 (53%; HMMER score = 30.8). This RPP8 MADA motif could substitute for the N-terminus of NRC4 indicating that it is functional (Figure 10). In Arabidopsis, RPP8 (AT5G43470) and its paralogs occur at dynamic genetic loci that exhibit frequent sequence exchanges as deduced from comparative genomic analyses (Kuang et al., 2008). Four of the five RPP8 paralogs in the Arabidopsis ecotype Col-0 were deemed to have a MADA motif based on our HMMER searches, whereas a fifth paralog LOV1 (AT1G10920) was negative and did not complement NRC4 autoactivity in the MADA motif swap experiments (Figure 10, Figure 10—figure supplement 1). LOV1 confers sensitivity to the victorin effector produced by the necrotrophic fungus *Cochliobolus victoriae* by binding the defense-associated thioredoxin TRX-h5 when it is complexed with victorin (Lorang et al., 2012). Interestingly, LOV1 binds TRX-h5 via its CC domain indicating that this region has evolved a pathogen sensor activity in this NLR protein (Lorang et al., 2012). How the sensor activity of the CC domain of LOV1 relates to the absence of a detectable MADA motif and whether this protein relies on other MADA-CC-NLRs to execute the cell death response are unanswered questions that are raised by these observations.

In activated ZAR1 resistosome, a funnel-shaped structure formed by five α1 helices is thought to directly execute hypersensitive cell death by forming a toxin-like pore in the plasma membrane (Wang et al., 2019b). To what extent do activated MADA-CC-NLRs function according to this ZAR1 model? Structure informed mutagenesis of ZAR1 revealed that F9, L10 and L14 on the outer surface of the funnel-shaped structure are required for immunity (Wang et al., 2019b). Here, our Ala and Glu scans of the MADA motif revealed that the NRC4 L9, L13 and L17 residues are essential for HR cell death activity. All three residues mapped to the outer surface of NRC4 α1 helices as predicted from a homology model based on the ZAR1 resistosome (Figure 8—figure supplement 2). We also found that mutations that perturb the MADA motif and prevent YFP self-association impair the capacity of $NRC4_{1-29}$-YFP to cause cell death and form puncta in *N. benthamiana* leaf cells (Figure 2—figure supplement 2, Figure 7—figure supplement 1, Figure 9). Our current interpretation of these results is that $NRC4_{1-29}$-YFP forms high-order complexes to cause cell death. However, direct support for this hypothesis is still missing. In addition, we lack detailed analyses of the cellular dynamics of the $NRC4_{1-29}$-YFP puncta and the degree to which they associate with membrane compartments in living plant cells. In the future, further biochemical, structural and cellular analyses are needed to determine the precise nature of the broadly conserved MADA motif and address the extent to which the ZAR1 “death switch” model occurs in CC-NLRs.

As discussed by Wang et al. (2019b), the interior space of the funnel structure is also important because the ZAR1 double mutant E11A/E18A is impaired in cell death and disease resistance activities. However, in our Glu mutant scan, we failed to observe a reduction in HR cell death activities with single site mutants in these residues or other amino acids that

are predicted to line up the interior space of the funnel-shaped structure. Whether or not this reflects genuine biological differences between ZAR1 and NRC4 remains to be studied.

A subset of CC-NLRs of the RPW8/HR family of atypical resistance proteins have a distinct type of coiled-coil domain known as CC_R (Barragan et al., 2019; Li et al., 2019). We failed to detect any MADA type sequences in these CC_R-NLR proteins. Indeed, the CC_R domain has similarity to mixed lineage kinase domain-like (MLKL) proteins and fungal HeLo/HELL domains, which form multi-helix bundles and act as membrane pore forming toxins (Barragan et al., 2019; Li et al., 2019; Mahdi et al., 2019). Whether the CC_R domains function as a distinct cell death inducing system in plants compared to MADA-CC-NLRs remains to be determined. Interestingly, Arabidopsis HR4, a CC_R containing protein, interacts in an allele-specific manner with the genetically unlinked CC-NLR RPP7b to trigger autoimmunity in the absence of pathogens (Barragan et al., 2019). Recently, Li et al. (2019) showed that RPP7b forms higher-order complexes of six to seven subunits only when activated by the matching autoimmune $HR4^{Fei-0}$ protein in a biochemical process reminiscent of activated ZAR1 resistosome (Li et al., 2019). In our HMMER searches, RPP7b and its four Arabidopsis paralogs were all classed as carrying the MADA motif. Thus, findings by Li et al. (2019) directly link a MADA-CC-NLR to the formation of resistosome type structures consistent with our view that the ZAR1 model widely applies to other NLRs with the MADA α1 helix. It will be fascinating to determine whether or not RPP7b and HR4 are both capable of executing cell death, especially as two-component systems of NLR and HeLo/HELL proteins are common in fungi and mammals (Barragan et al., 2019).

Plant NLRs can be functionally categorized into singleton, sensor or helper NLRs based on their biological activities (Adachi et al., 2019a). However, it remains challenging to predict NLR functions from the wealth of unclassified NLRomes that are emerging from plant genome sequences. It has not escaped our attention that the discovery of the MADA motif as a signature of NLR singletons and helpers—but missing in sensor NLRs—enables the development of computational pipelines for predicting NLR networks from naïve plant genomes. Such *in silico* predictions can be tested by co-expression of paired NLRs in *N. benthamiana*. In addition, MADA motif predictions can be validated using our straightforward functional assay of swapping the NRC4 N-terminus, with the readouts consisting of both HR cell death (Figure 10) and resistance to *P. infestans* (Figure 11). Dissecting the NLR network architecture of plant species is not only useful for basic mechanistic studies but has also direct implications for breeding disease resistance into crop plants and reducing the autoimmune load of NLRs (Chae et al., 2016; Wu et al., 2018; Adachi et al., 2019a).

Materials and Methods

Key Resources Table				
Reagent type (species) or resource	**Designation**	**Source or reference**	**Identifiers**	**Additional information**

Genetic reagent (*Nicotiana benthamiana*)	NRC4-KO *N. benthamiana* (*nrc4a/b_9.1.3* and *nrc4a/b_1.2.1*)	This paper		Materials and Methods: Generation of *N. benthamiana nrc4a/b* CRISPR/Cas9 mutants
Recombinant DNA reagent	pGEM::Mu-STOP	This paper		Materials and Methods: Mu-STOP *in vitro* transposition
Commercial assay, kit	Mutation Generation System Kit	Thermo Fisher	Cat #: F-701	Materials and Methods: Mu-STOP *in vitro* transposition
Gene (*Solanum lycopersicum*)	Tomato genome sequence (Tomato ITAG release 2.40)	Sol Genomics Network (https://solgenomics.net/)		Materials and Methods: Bioinformatic and phylogenetic analyses
Gene (*N. benthamiana*)	*N. benthamiana* genome sequence (*N. benthamiana* Genome v0.4.4)	Sol Genomics Network (https://solgenomics.net/)		Materials and Methods: Bioinformatic and phylogenetic analyses
Gene (*Arabidopsis thaliana*)	Arabidopsis genome sequence (Araport11)	https://www.araport.org/		Materials and Methods: Bioinformatic and phylogenetic analyses
Gene (*Beta vulgaris*)	Sugar beet genome sequence (RefBeet-1.2)	http://bvseq.molgen.mpg.de/index.shtml		Materials and Methods: Bioinformatic and phylogenetic analyses
Gene (*Oryza sativa*)	Rice genome sequence (Rice Gene Models in Release 7)	http://rice.plantbiology.msu.edu/		Materials and Methods: Bioinformatic and phylogenetic analyses
Gene (*Hordeum vulgare*)	Barley genome sequence (IBSC_v2)	https://www.barleygenome.org.uk/		Materials and Methods: Bioinformatic and phylogenetic analyses

Other	3D structure of ZAR1	Protein Data Bank	6J5T	Materials and Methods: Structure homology modelling

Plant growth conditions

Wild type and mutant *N. benthamiana* were propagated in a glasshouse and, for most experiments, were grown in a controlled growth chamber with temperature 22-25°C, humidity 45-65% and 16/8-h light/dark cycle.

Generation of *N. benthamiana nrc4a/b* CRISPR/Cas9 mutants

Constructs for generating *NRC4* knockout *N. benthamiana* were assembled using the Golden Gate cloning method (Weber et al., 2011; Nekrasov et al., 2013; Belhaj et al., 2013). sgRNA4.1 and sgRNA4.2 were cloned under the control of the Arabidopsis (*Arabidopsis thaliana*) U6 promoter (AtU6pro) [pICSL90002, The Sainsbury Laboratory (TSL) SynBio] and assembled in pICH47751 (Addgene no. 48002) and pICH47761 (Addgene no. 48003), respectively as previously described (Belhaj et al., 2013). Primers sgNbNRC4.1_F (tgtggtctcaATTGAAAAACGGTACATACCGCAGgttttagagctagaaatagcaag), sgNbNRC4.2_F (tgtggtctcaATTGAGTCAGGAATCTTGCAGCTGgttttagagctagaaatagcaag) and sgRNA_R (tgtggtctcaAGCGTAATGCCAACTTTGTAC) were used to clone sgRNA4.1 and sgRNA4.2. pICSL11017::NOSpro::BAR (TSL SynBio), pICSL11021::35Spro::Cas9 (Addgene no. 49771), pICH47751::AtU6p::sgRNA4.1, pICH47761::AtU6pro::sgRNA4.2, and the linker pICH41780 (Addgene no. 48019) were assembled into the vector pICSL4723 (Addgene no. 48015) as described (Weber et al., 2011) resulting in construct pICSL4723::BAR::Cas9::sgRNA4.1::sgRNA4.2 that was used for plant transformation. Transgenic *N. benthamiana* were generated by TSL Plant Transformation team as described before (Nekrasov et al., 2013).

***N. benthamiana nrc4a/b* genotyping**

Genomic DNA of selected T2 *N. benthamiana* transgenic plants *nrc4a/b*_9.1.3 and *nrc4a/b*_1.2.1 was extracted using DNeasy Plant DNA Extraction Kit (Qiagen). Primers NRC4_1_F (GGAAGTGCAAAGGGAGAGTT), NRC4_1_R (TCGCCTGAACCACAAACTTA), NRC4_2_F (GGCAAGAATTTTGGATGTGG) and NRC4_2_R (CGAGGAACCCTTTTTAGGCAG) were used in multiplex polymerase chain reaction (PCR) assays to amplify the region targeted by the two sgRNAs. Multiplex amplicon sequencing was performed by the Hi-Plex technique (Lyon et al., 2016). Sequence reads were aligned to the reference *N. benthamiana* draft genome Niben.genome.v0.4.4 [Sol Genomics Network (SGN), https://solgenomics.net/], and *NRC4a* (on scaffold Niben044Scf00002971) and *NRC4b* (on scaffold Niben044Scf00016103) were further analysed. T3 lines from the selected T2 plants were used for the experiments.

Plasmid constructions

To generate $NRC4_{1\text{-}29}$-YFP expression construct, $NRC4_{1\text{-}29}$ coding sequence was amplified by Phusion High-Fidelity DNA Polymerase (Thermo Fisher), and the purified amplicon was directly used in Golden Gate assembly with pICH85281 [mannopine synthase promoter+Ω (MasΩpro), Addgene no. 50272], pICSL50005 (YFP, TSL SynBio), pICSL60008 [Arabidopsis heat shock protein terminator (HSPter), TSL SynBio] into binary vector pICH47742 (Addgene no. 48001). Primers used for $NRC4_{1\text{-}29}$ coding sequences are listed in Supplementary file 1.

To generate an autoactive mutant of *N. benthamiana* NRC4, the aspartic acid (D) in the MHD motif was substituted to valine (V) by site-directed mutagenesis using Phusion High-Fidelity DNA Polymerase (Thermo Fisher). pCR8::$NRC4^{WT}$ (Wu et al., 2017) was used as a template. Primers NRC4_D478V_F (5'-Phos/ATGTTGCATCAGTTCTGCAAAAAGGAGGCT) and NRC4_D478V_R (5'-Phos/GACGTGAAGACGACATGTTTTTATTTGACC) were used for introducing the mutation in the PCR. The mutated NRC4 was verified by DNA sequencing of the obtained plasmid.

pCR8::$NRC4^{WT}$ (Wu et al., 2017) or pCR8::$NRC4^{DV}$ without its stop codon were used as a level 0 modules for the following Golden Gate cloning. $NRC4^{DV}$-3xFLAG was generated by Golden Gate assembly with pICH51266 [35S promoter+Ω promoter, Addgene no. 50267], pICSL50007 (3xFLAG, Addgene no. 50308) and pICH41432 (octopine synthase terminator, Addgene no. 50343) into binary vector pICH47732 (Addgene no. 48000). $NRC4^{WT}$-6xHA and $NRC4^{DV}$-6xHA were generated by Golden Gate assembly with pICH85281 (MasΩpro), pICSL50009 (6xHA, Addgene no. 50309), pICSL60008 (HSPter) into the binary vector pICH47742. $NRC4^{WT}$-YFP and $NRC4^{DV}$-YFP were generated by Golden Gate assembly with pICH85281 (MasΩpro), pICSL50005 (YFP), pICSL60008 (HSPter) into binary vector pICH47742. For free YFP expression construct, pAGM3212 (YFP, TSL SynBio) was assembled with pICH85281 (MasΩpro) and pICSL60008 (HSPter) into the binary vector pICH47742 by Golden Gate reaction.

To reduce homo-affinity of YFP, YFP alanine (A) 206 was substituted to lysine (K) (Zacharias et al., 2002), by site-directed mutagenesis using Phusion High-Fidelity DNA Polymerase (Thermo Fisher). pAGM3212 (YFP, TSL SynBio) was used as a template. Primers used for mutagenesis are listed in Supplementary file 1. The amplicons were directly used in Golden Gate assembly with pICH41308 (Addgene no. 47998) or pAGM1301 (Addgene no. 47989). pICH41308::YFP^{A206K} was assembled with pICH85281 (MasΩpro) and pICSL60008 (HSPter) into the binary vector pICH47742 by Golden Gate reaction. pAGM1301::YFP^{A206K} was assembled with pCR8::$NRC4^{DV}$ or $NRC4_{1\text{-}29}$ amplicon, pICH85281 (MasΩpro) and pICSL60008 (HSPter) into the binary vector pICH47742 by Golden Gate reaction.

To generate MADA motif mutants and chimeras of NRC4, the full-length sequence of $NRC4^{WT}$ or $NRC4^{DV}$ was amplified by Phusion High-Fidelity DNA Polymerase (Thermo Fisher) with the forward primers listed in Supplementary file 1. Purified amplicons were cloned into pCR8/GW/D-TOPO (Invitrogen) as a level 0 module. The level 0 plasmids were then used for Golden Gate assembly with pICH85281 (MasΩpro), pICSL50009 (6xHA) and pICSL60008 (HSPter) into the binary vector pICH47742.

To generate pTRBO::YFP, pTRBO::$ZAR1_{1\text{-}144}$-YFP, pTRBO::$ZAR1_{1\text{-}144}{}^{F9A/L10A/L14A}$-YFP, pTRBO::$NRC4_{1\text{-}29}$-YFP and pTRBO::$NRC4_{1\text{-}29}{}^{L9A/V10A/L14A}$-YFP plasmids, we used GENEWIZ

Standard Gene Synthesis with custom vector cloning service into the pTRBO vector (Lindbo, 2007a).

Mu-STOP *in vitro* transposition

To generate the Mu-STOP transposon (Poussu et al., 2005), entranceposon M1-KanR (Mutation Generation System Kit, Thermo Fisher) was used as a PCR template, and three translational stop signals were added to each transposon end by Phusion High-Fidelity DNA Polymerase and Mu-STOP primer (GGAAGATCTGATTGATTGAACGAAAAACGCGAAAGCGTTTC). The 3' A overhang was then introduced to the Mu-STOP amplicon by DreamTaq DNA polymerase (Thermo Fisher), and the resulting Mu-STOP amplicon was cloned into pGEM-T Easy (Promega). Mu-STOP transposon was then released from pGEM::Mu-STOP by *Bgl*II digestion and purified by GeneJET Gel Extraction Kit (Thermo Fisher). 100 ng of the purified Mu-STOP transposon was mixed with 500 ng of the target plasmid, pICH47732::35SΩpro::NRC4^{DV}-3xFLAG, and MuA transposase from the Mutation Generation System Kit (Thermo Fisher). The *in vitro* transposition reaction was performed according to the manufacturer's procedure and carried out at 30°C for 6 hours.

The NRC4^{DV}::Mu-STOP library was transformed into *Agrobacterium tumefaciens* Gv3101 by electroporation. Mu-STOP insertion sites were determined by colony PCR using DreamTaq DNA polymerase (Thermo Fisher) and PCR amplicon sequencing. For the PCR, we used a forward primer (GAACCCTGTGGTTGGCATGCACATAC) matching pICH47732 and a reverse primer (CAACGTGGCTTACTAGGATC) matching Mu-STOP transposon.

Transient gene-expression and cell death assays

Transient expression of NRC wild-type and mutants, as well as other genes, in *N. benthamiana* were performed by agroinfiltration according to methods described by Bos et al. (2006). Briefly, four-weeks old *N. benthamiana* plants were infiltrated with *A. tumefaciens* strains carrying the binary expression plasmids. *A. tumefaciens* suspensions were prepared in infiltration buffer (10 mM MES, 10 mM $MgCl_2$, and 150 µM acetosyringone, pH5.6) and were adjusted to OD_{600} = 0.5. For transient expression of NRC4^{WT}-YFP, NRC4^{DV}-YFP, NRC4$_{1\text{-}29}$-YFP, free YFP and the YFP^{A206K} variants, the *A. tumefaciens* suspensions (OD_{600} = 0.25) were mixed in a 1:1 ratio with an *A. tumefaciens* expressing p19, the suppressor of posttranscriptional gene silencing of *Tomato bushy stunt virus* that is known to enhance *in planta* protein expression (Lindbo, 2007b). HR cell death phenotypes were scored according to the scale of Segretin et al. (2014) modified to range from 0 (no visible necrosis) to 7 (fully confluent necrosis). In Figure 2—figure supplement 2 and Figure 7—figure supplement 1, cell death was visualized with Odyssey Infrared Imager (800 nm channel, LI-COR).

Protein immunoblotting

Protein samples were prepared from six discs (8 mm diameter) cut out of *N. benthamiana* leaves at 1 day after agroinfiltration and were homogenised in extraction buffer [10% glycerol, 25 mM Tris-HCl, pH 7.5, 1 mM EDTA, 150 mM NaCl, 2% (w/v) PVPP, 10 mM DTT, 1x

protease inhibitor cocktail (SIGMA), 0.2% IGEPAL (SIGMA)]. The supernatant obtained after centrifugation at 12,000 x*g* for 10 min was used for SDS-PAGE. Immunoblotting was performed with HA-probe (F-7) HRP (Santa Cruz Biotech) or anti-GFP antibody (ab290, abcam) in a 1:5,000 dilution. Equal loading was checked by taking images of the stained PVDF membranes with Pierce Reversible Protein Stain Kit (#24585, Thermo Fisher).

Bioinformatic and phylogenetic analyses

We used NLR-parser (Steuernagel et al., 2015) to identify NLR sequences from the protein databases of tomato (SGN, Tomato ITAG release 2.40), *N. benthamiana* (SGN, *N. benthamiana* Genome v0.4.4), Arabidopsis (https://www.araport.org/, Araport11), sugar beet (http://bvseq.molgen.mpg.de/index.shtml, RefBeet-1.2), rice (http://rice.plantbiology.msu.edu/, Rice Gene Models in Release 7) and barley (https://www.barleygenome.org.uk/, IBSC_v2). The obtained NLR sequences, from NLR-parser, were aligned using MAFFT v. 7 (Katoh and Standley, 2013), and the protein sequences that lacked the p-loop motif were discarded from the NLR dataset. The gaps in the alignments were deleted manually in MEGA7 (Kumar et al., 2016) and the NB-ARC domains were used for generating phylogenetic trees (Figure 3—figure supplement 1—source data 1). The neighbour-joining tree was made using MEGA7 with JTT model and bootstrap values based on 100 iterations (Figure 3—figure supplement 1). We removed TIR-NLR clade members from the final database, and retained all CC-NLR sequences, including the CC_R-NLR (RPW8-NLR), that possess N-terminal domains longer than 30 amino acids (988 protein sequences, Figure 3—source data 1).

The NB-ARC domain sequences from 988 proteins (Figure 3—figure supplement 2—source data 1) were used to construct the CC-NLR phylogenetic tree in Figure 3—figure supplement 2. The neighbour-joining tree was constructed as described above.

For the tribe analyses, we extracted the N-terminal domain sequences, prior to NB-ARC domain, from the CC-NLR database (Figure 3—source data 2), and used the Tribe-MCL feature from Markov Cluster Algorithm (Enright et al., 2002) to cluster the sequences into tribes with BLASTP E-value cutoff < 10^{-8}. NLRs in each tribe were subjected to motif searches using the MEME (Multiple EM for Motif Elicitation) v. 5.0.5 (Bailey and Elkan, 1994) with parameters “zero or one occurrence per sequence, top 5 motifs”, to detect consensus motifs conserved in >= 70% of input sequences.

We used the most N-terminal motif detected in Tribe 2 from the MEME analysis to construct a hidden Markov model (HMM) for the MADA motif. Sequences aligned to the MADA motif were extracted in Stockholm format and used in hmmbuild program implemented in HMMER v2.3.2 (Eddy, 1998). The HMM was then calibrated with hmmcalibrate. This MADA-HMM (Supplementary file 2) was used to search the CC-NLR database (Figure 3—source data 1) with the hmmsearch program (hmmsearch --max -o <outputfile> <hmmfile> <seqdb>). To estimate the false positive rate, hmmsearch program was applied to full Arabidopsis and tomato proteomes (Araport11 and ITAG3.2) with the MADA-HMM and the output is displayed in Figure 4—source data 2 and discussed in the results section.

Pathogen infection assays

P. infestans infection assays were performed by applying droplets of zoospore suspension on detached leaves as described previously (Song et al., 2009). Briefly, leaves of five-weeks old wild-type and *nrc4a/b N. benthamiana* plants were infiltrated with *A. tumefaciens* solutions, in which each *Agrobacterium* containing a plasmid expressing RFP::Rpi-blb2 (Wu et al., 2017) was mixed in a 1:1 ratio (OD_{600} = 0.5 for each strain) with *Agrobacterium* containing either the empty vector, wild type NRC4, or NRC4 variant. At 24 hours after agroinfiltration, the abaxial side of the leaves were inoculated with 10 µL zoospore suspension (100 zoospores/µL) of *P. infestans* strain 88069 prepared according to the methods reported by Song et al. (2009). The inoculated leaves were kept in a moist chamber at room temperature (21-24°C) for 7 days, and imaged under UV light (UVP Blak-Ray B-100AP lights – 365nm) with Wratten No.8 Yellow Filter for visualization of the lesions. The camera setting was ISO 1600, White Balance 6250K, F11 and 10 sec exposure.

Structure homology modelling

We used the cryo-EM structure of activated ZAR1 (Wang et al. 2019b) as template to generate a homology model of NRC4. The amino acid sequence of NRC4 was submitted to Protein Homology Recognition Engine V2.0 (Phyre2) for modelling (Kelley et a., 2015). The coordinates of ZAR1 structure (6J5T) were retrieved from the Protein Data Bank and assigned as modelling template by using Phyre2 Expert Mode. The resulting model of NRC4 comprised amino acids Val-5 to Glu-843 and was illustrated in CCP4MG software (McNicholas et al., 2011).

Microscopy

For localization analyses, leaf discs (6 mm in diameter) of *N. benthamiana* leaves were made 2 days after agroinfiltration and were used for imaging. Images were captured with Leica SP8 resonant inverted confocal microscope (Leica Microsystems). For excitation, Argon laser and Helium-Neon laser wer set to 514 nm and 633 nm, respectively. Hybrid detectors were used with 517–575 and 584–638 nm bandpass filters to capture YFP and RFP signals, respectively. Gain, laser intensities and zoom were kept the same for all images. Images were processed in FIJI (Fiji Is Just ImageJ).

Accession Numbers

The NRC4 sequences used in this study can be found in the Solanaceae Genomics Network (SGN) or GenBank/EMBL databases with the following accession numbers: NbNRC4 (NbNRC4, MK692737; NbNRC4a, Niben044Scf00002971; NbNRC4b, Niben044Scf00016103).

Acknowledgements

We are thankful to several colleagues for discussions and ideas. We thank Matthew Smoker and other members of the TSL Plant Transformation facility as well as Mark Youles of TSL SynBio for invaluable technical support. We thank Kurt Lamour for advice on genotyping the

CRISPR/Cas9 mutants. H.A. is funded by the Japan Society for the Promotion of Science (JSPS) and L.D. by a Marie Sklodowska-Curie Actions (MSCA) Fellowship. The Kamoun Lab is funded primarily from the Gatsby Charitable Foundation, Biotechnology and Biological Sciences Research Council (BBSRC, UK), and European Research Council (ERC; NGRB and BLASTOFF projects).

Declaration of interests

S.K., L.D. and C.H.-W. filed a patent on NRCs (WO/2019/108619). S.K. receives funding from industry on NLR biology.

References

Adachi H, Derevnina L, Kamoun S. 2019a. NLR singletons, pairs, and networks: evolution, assembly, and regulation of the intracellular immunoreceptor circuitry of plants. *Curr Opin Plant Biol* **50**:121-131. doi: 10.1016/j.pbi.2019.04.007.

Adachi H, Kamoun S, Maqbool A. 2019b. A resistosome-activated 'death switch'. *Nat Plants* **5**:457-458. doi: 10.1038/s41477-019-0425-9.

Bailey TL, Elkan C. 1994. Fitting a mixture model by expectation maximization to discover motifs in biopolymers. *Proc Int Conf Intell Syst Mol Biol* **2**:28-36.

Barragan C, Wu R, Kim S-T, Xi W, Habring A, Hagmann J, Van de Weyer A-L, Zaidem M, Ho WWH, Wang G, Bezrukov I, Weigel D, Chae E. 2019. RPW8/HR repeats control NLR activation in *Arabidopsis thaliana*. *PLoS Genet* **15**:e1008313. doi: 10.1371/journal.pgen.1008313.

Baudin M, Hassan JA, Schreiber KJ, Lewis JD. 2017. Analysis of the ZAR1 immune complex reveals determinants for immunity and molecular interactions. *Plant Physiol* **174**:2038-2053. doi: 10.1104/pp.17.00441.

Belhaj K, Chaparro-Garcia A, Kamoun S, Nekrasov V. 2013. Plant genome editing made easy: targeted mutagenesis in model and crop plants using the CRISPR/Cas system. *Plant Methods* **9**:39. doi: 10.1186/1746-4811-9-39.

Bentham AR, Zdrzalek R, De la Concepcion JC, Banfield MJ. 2018. Uncoiling CNLs: Structure/function approaches to understanding CC domain function in plant NLRs. *Plant Cell Physiol* **59**:2398-2408. doi: 10.1093/pcp/pcy185.

Białas A, Zess EK, De la Concepcion JC, Franceschetti M, Pennington HG, Yoshida K, Upson JL, Chanclud E, Wu CH, Langner T, Maqbool A, Varden FA, Derevnina L, Belhaj K, Fujisaki K, Saitoh H, Terauchi R, Banfield MJ, Kamoun S. 2018. Lessons in effector and NLR biology of plant-microbe systems. *Mol Plant Microbe Interact* **31**:34-45. doi: 10.1094/MPMI-08-17-0196-FI.

Bonardi V, Tang S, Stallmann A, Roberts M, Cherkis K, Dangl JL. 2011. Expanded functions for a family of plant intracellular immune receptors beyond specific recognition of pathogen effectors. *Proc Natl Acad Sci U S A* **108**:16463-16468. doi: 10.1073/pnas.1113726108.

Bos JI, Kanneganti TD, Young C, Cakir C, Huitema E, Win J, Armstrong MR, Birch PR, Kamoun S. 2006. The C-terminal half of *Phytophthora infestans* RXLR effector AVR3a is sufficient to trigger R3a-mediated hypersensitivity and suppress INF1-induced cell death in *Nicotiana benthamiana*. *Plant J* **48**:165-176. doi: 10.1111/j.1365-313X.2006.02866.x.

Bozkurt TO, Richardson A, Dagdas YF, Mongrand S, Kamoun S, Raffaele S. 2014. The plant membrane-associated REMORIN1.3 accumulates in discrete perihaustorial domains and enhances susceptibility to *Phytophthora infestans*. *Plant Physiol* **165**:1005-1018. doi: 10.1104/pp.114.235804.

Casey LW, Lavrencic P, Bentham AR, Cesari S, Ericsson DJ, Croll T, Turk D, Anderson PA, Mark AE, Dodds PN, Mobli M, Kobe B, Williams SJ. 2016. The CC domain structure from the wheat stem rust resistance protein Sr33 challenges paradigms for dimerization in plant NLR proteins. *Proc Natl Acad Sci U S A* **113**:12856-12861. doi: 10.1073/pnas.1609922113.

Castel B, Ngou PM, Cevik V, Redkar A, Kim DS, Yang Y, Ding P, Jones JDG. 2019. Diverse NLR immune receptors activate defence via the RPW8-NLR NRG1. *New Phytol* **222**:966-980. doi: 10.1111/nph.15659.

Cesari S, Moore J, Chen C, Webb D, Periyannan S, Mago R, Bernoux M. 2016. Cytosolic activation of cell death and stem rust resistance by cereal MLA-family CC–NLR proteins. *Proc Natl Acad Sci U S A* **113**:10204-10209. doi: 10.1073/pnas.1605483113.

Chae E, Tran DT, Weigel D. 2016. Cooperation and conflict in the plant immune system. *PLoS Pathog* **12**:e1005452. doi: 10.1371/journal.ppat.1005452.

Collier SM, Hamel LP, Moffett P. 2011. Cell death mediated by the N-terminal domains of a unique and highly conserved class of NB-LRR protein. *Mol Plant Microbe Interact* **24**:918-231. doi: 10.1094/MPMI-03-11-0050.

Dodds PN, Rathjen JP. 2010. Plant immunity: towards an integrated view of plant-pathogen interactions. *Nat Rev Genet* **11**:539-548. doi: 10.1038/nrg2812.

Dong OX, Tong M, Bonardi V, El Kasmi F, Woloshen V, Wünsch LK, Dangl JL, Li X. 2016. TNL-mediated immunity in *Arabidopsis* requires complex regulation of the redundant *ADR1* gene family. *New Phytol* **210**:960-973. doi: 10.1111/nph.13821.

Enright AJ, Van Dongen S, Ouzounis CA. 2002. An efficient algorithm for large-scale detection of protein families. *Nucleic Acids Res* **30**:1575-1584. doi: 10.1093/nar/30.7.1575.

Eddy SR. 1998. Profile hidden Markov models. *Bioinformatics* **14**:755-763. doi: 10.1093/bioinformatics/14.9.755.

Hu Z, Zhou Q, Zhang C, Fan S, Cheng W, Zhao Y, Shao F, Wang HW, Sui SF, Chai J. 2015. Structural and biochemical basis for induced self-propagation of NLRC4. *Science* **350**:399-404. doi: 10.1126/science.aac5489.

Jones JDG, Vance RE, Dangl JL. 2016. Intracellular innate immune surveillance devices in plants and animals. *Science* **354**. doi: 10.1126/science.aaf6395.

Jubic LM, Saile S, Furzer OJ, El Kasmi F, Dangl JL. 2019. Help wanted: helper NLRs and plant immune responses. *Curr Opin Plant Biol* **50:**82-94. doi: 10.1016/j.pbi.2019.03.013.

Katoh K, Standley DM. 2013. MAFFT multiple sequence alignment software version 7: improvements in performance and usability. *Mol Biol Evol* **30**:772-780. doi: 10.1093/molbev/mst010.

Kelley LA, Mezulis S, Yates CM, Wass MN, Sternberg MJ. 2015. The Phyre2 web portal for protein modeling, prediction and analysis. *Nat Protoc* **10**:845-858. doi: 10.1038/nprot.2015.053.

Kim YE, Kim YN, Kim JA, Kim HM, Jung Y. 2015. Green fluorescent protein nanopolygons as monodisperse supramolecular assemblies of functional proteins with defined valency. *Nat Commun* **6**:7134. doi: 10.1038/ncomms8134.

Kuang H, Caldwell KS, Meyers BC, Michelmore RW. 2008. Frequent sequence exchanges between homologs of *RPP8* in Arabidopsis are not necessarily associated with genomic proximity. *Plant J* **54**:69-80. doi: 10.1111/j.1365-313X.2008.03408.x.

Kourelis J, van der Hoorn RAL. 2018. Defended to the nines: 25 years of resistance gene cloning identifies nine mechanisms for R protein function. *Plant Cell* **30**:285-299. doi: 10.1105/tpc.17.00579.

Kumar S, Stecher G, Tamura K. 2016. MEGA7: molecular evolutionary genetics analysis version 7.0 for bigger datasets. *Mol Biol Evol* **33**:1870-1874. doi: 10.1093/molbev/msw054.

Li J, Huang H, Zhu M, Huang S, Zhang W, Dinesh-Kumar SP, Tao X. 2019. A Plant Immune Receptor Adopts a Two-Step Recognition Mechanism to Enhance Viral Effector Perception. *Mol Plant* **12**:248-262. doi: 10.1016/j.molp.2019.01.005.

Li L, Habring A, Wang K, Weigel D. 2019. Oligomerization of NLR immune receptor RPP7 triggered by atypical resistance protein RPW8/HR as ligand. *bioRxiv* doi: https://doi.org/10.1101/682807.

Lindbo JA. 2007a. TRBO: a high-efficiency tobacco mosaic virus RNA-based overexpression vector. *Plant Physiol* **145**:1232-1240. doi: 10.1104/pp.107.106377.

Lindbo JA. 2007b. High-efficiency protein expression in plants from agroinfection-compatible *Tobacco mosaic virus* expression vectors. *BMC Biotechnol* **7**:52. doi:10.1186/1472-6750-7-52.

Lorang J, Kidarsa T, Bradford CS, Gilbert B, Curtis M, Tzeng SC, Maier CS, Wolpert TJ. 2012. Tricking the guard: exploiting plant defense for disease susceptibility. *Science* **338**:659-662. doi: 10.1126/science.1226743.

Lyon R, Correll J, Feng C, Bluhm B, Shrestha S, Shi A, Lamour K. 2016. Population structure of *Peronospora effusa* in the southwestern United States. *PLoS One* **11**:e0148385. doi: 10.1371/journal.pone.0148385.

Maekawa T, Cheng W, Spiridon LN, Töller A, Lukasik E, Saijo Y, Liu P, Shen QH, Micluta MA, Somssich IE, Takken FLW, Petrescu AJ, Chai J, Schulze-Lefert P. 2011. Coiled-coil domain-dependent homodimerization of intracellular barley immune receptors defines a minimal functional module for triggering cell death. *Cell Host Microbe* **9**:187-199. doi: 10.1016/j.chom.2011.02.008.

Mahdi L, Huang M, Zhang X, Nakano RT, Kopp LB, Saur IML, Jacob F, Kovacova V, Lapin D, Parker JE, Murphy JM, Hofmann K, Schulze-Lefert P, Chai J, Maekawa T. 2019. Plant mixed lineage kinase domain-like proteins limit biotrophic pathogen growth. *bioRxiv* doi: https://doi.org/10.1101/681015.

Maqbool A, Saitoh H, Franceschetti M, Stevenson CEM, Uemura A, Kanzaki H, Kamoun S, Terauchi R, Banfield MJ. 2015. Structural basis of pathogen recognition by an integrated HMA domain in a plant NLR immune receptor. *Elife* **4**:1-24. doi: 10.7554/eLife.08709.

McNicholas S, Potterton E, Wilson KS, Noble ME. 2011. Presenting your structures: the CCP4mg molecular-graphics software. *Acta Crystallogr D Biol Crystallogr* **67**:386-394. doi: 10.1107/S0907444911007281.

Nekrasov V, Staskawicz B, Weigel D, Jones JD, Kamoun S. 2013. Targeted mutagenesis in the model plant *Nicotiana benthamiana* using Cas9 RNA-guided endonuclease. *Nat Biotechnol* **31**:691-693. doi: 10.1038/nbt.2655.

Oh SK, Young C, Lee M, Oliva R, Bozkurt TO, Cano LM, Win J, Bos JI, Liu HY, van Damme M, Morgan W, Choi D, Van der Vossen EA, Vleeshouwers VG, Kamoun S. 2009. In planta expression screens of *Phytophthora infestans* RXLR effectors reveal diverse phenotypes, including activation of the *Solanum bulbocastanum* disease resistance protein Rpi-blb2. *Plant Cell* **21**:2928-2947. doi: 10.1105/tpc.109.068247.

Peart JR, Mestre P, Lu R, Malcuit I, Baulcombe DC. 2005. NRG1, a CC-NB-LRR protein, together with N, a TIR-NB-LRR protein, mediates resistance against tobacco mosaic virus. *Curr Biol* **15**:968-973. doi: 10.1016/j.cub.2005.04.053.

Poussu E, Jäntti J, Savilahti H. 2005. A gene truncation strategy generating N- and C-terminal deletion variants of proteins for functional studies: mapping of the Sec1p binding domain in yeast Mso1p by a Mu *in vitro* transposition-based approach. *Nucleic Acids Res* **33**:e104. doi: 10.1093/nar/gni102.

Qi S, Pang Y, Hu Q, Liu Q, Li H, Zhou Y, He T, Liang Q, Liu Y, Yuan X, Luo G, Li H, Wang J, Yan N, Shi Y. 2010. Crystal structure of the *Caenorhabditis elegans* apoptosome reveals an octameric assembly of CED-4. *Cell* **141**:446-457. doi: 10.1016/j.cell.2010.03.017.

Qi T, Seong K, Thomazella DPT, Kim JR, Pham J, Seo E, Cho M-J, Schultink A, Staskawicz BJ. 2018. NRG1 functions downstream of EDS1 to regulate TIR-NLR-mediated plant immunity in *Nicotiana benthamiana*. *Proc Natl Acad Sci U S A* **115**:E10979-E10987. doi: 10.1073/pnas.1814856115.

Rairdan GJ, Collier SM, Sacco MA, Baldwin TT, Boettrich T, Moffett P. 2008. The coiled-coil and nucleotide binding domains of the potato Rx disease resistance protein function in pathogen recognition and signaling. *Plant Cell* **20**:739-751. doi: 10.1105/tpc.107.056036.

Segretin ME, Pais M, Franceschetti M, Chaparro-Garcia A, Bos JI, Banfield MJ, Kamoun S. 2014. Single amino acid mutations in the potato immune receptor R3a expand response to *Phytophthora* effectors. *Mol Plant Microbe Interact* **27**:624-637. doi: 10.1094/MPMI-02-14-0040-R.

Saur IM, Conlan BF, Rathjen JP. 2015. The N-terminal domain of the tomato immune protein Prf contains multiple homotypic and Pto kinase interaction sites. *J Biol Chem* **290**:11258-11267. doi: 10.1074/jbc.M114.616532.

Shao Z-Q, Xue J-Y, Wu P, Zhang Y-M, Wu Y, Hang Y-Y, Wang B, Chen J-Q. 2016. Large-scale analyses of angiosperm nucleotide-binding site-leucine-rich repeat genes reveal three anciently diverged classes with distinct evolutionary patterns. *Plant Physiol* **170**:2095-2109. doi: 10.1104/pp.15.01487.

Song J, Win J, Tian M, Schornack S, Kaschani F, Ilyas M, van der Hoorn RA, Kamoun S. 2009. Apoplastic effectors secreted by two unrelated eukaryotic plant pathogens target the tomato defense protease Rcr3. *Proc Natl Acad Sci U S A* **106**:1654-1659. doi: 10.1073/pnas.0809201106.

Stam R, Silva-Arias GA, Tellier A. 2019. Subsets of *NLR* genes show differential signatures of adaptation during colonisation of new habitats. *New Phytol* **22**. doi: 10.1111/nph.16017.

Steuernagel B, Jupe F, Witek K, Jones JD, Wulff BB. 2015. NLR-parser: rapid annotation of plant NLR complements. *Bioinformatics* **31**:1665-1667. doi: 10.1093/bioinformatics/btv005.

Steuernagel B, Witek K, Krattinger SG, Ramirez-Gonzalez RH, Schoonbeek H-J, Yu G, Baggs E, Witek AI, Yadav I, Krasileva KV, Jones JDG, Uauy C, Keller B, Ridout CJ, The International Wheat Genome Sequencing Consortium, Wulff BB. 2018. Physical and transcriptional organisation of the bread wheat intracellular immune receptor repertoire. *bioRxiv* doi: https://doi.org/10.1101/339424.

Tenthorey JL, Haloupek N, López-Blanco JR, Grob P, Adamson E, Hartenian E, Lind NA, Bourgeois NM, Chacón P, Nogales E, Vance RE. 2017. The structural basis of flagellin detection by NAIP5: A strategy to limit pathogen immune evasion. *Science* **358**:888-893. doi: 10.1126/science.aao1140.

van der Vossen E, Sikkema A, Hekkert Bt, Gros J, Stevens P, Muskens M, Wouters D, Pereira A, Stiekema W, Allefs S. 2003. An ancient *R* gene from the wild potato species *Solanum bulbocastanum* confers broad-spectrum resistance to *Phytophthora infestans* in cultivated potato and tomato. *Plant J* **36**:867-882. doi: 10.1046/j.1365-313X.2003.01934.x.

Wang GF, Ji J, El-Kasmi F, Dangl JL, Johal G, Balint-Kurti PJ. 2015. Molecular and functional analyses of a maize autoactive NB-LRR protein identify precise structural requirements for activity. *PLoS Pathog* **26**:e1004674. doi: 10.1371/journal.ppat.1004674.

Wang J, Wang J, Hu M, W Shan, Qi J, Wang G, Han Z, Qi Y, Gao N, Wang H-W, Zhou J-M, Chai J. 2019a. Ligand-triggered allosteric ADP release primes a plant NLR complex. *Science* **364**:eaav5868. doi: 10.1126/science.aav5868.

Wang J, Hu M, Wang J, Qi J, Han Z, Wang G, Qi Y, Wang H-W, Zhou J-M, Chai J. 2019b. Reconstitution and structure of a plant NLR resistosome conferring immunity. *Science* **364**:eaav5870. doi: 10.1126/science.aav5870.

Weber E, Engler C, Gruetzner R, Werner S, Marillonnet S. 2011. A modular cloning system for standardized assembly of multigene constructs. *Plos One* **6**:e16765. doi: 10.1371/journal.pone.0016765.

Wu C-H, Derevnina L, Kamoun S. 2018. Receptor networks underpin plant immunity. *Science* **360:**1300-1301. doi: 10.1126/science.aat2623.

Wu C-H, Abd-El-Haliem A, Bozkurt TO, Belhaj K, Terauchi R, Vossen JH, Kamoun S. 2017. NLR network mediates immunity to diverse plant pathogens. *Proc Natl Acad Sci U S A* **114**:8113-8118. doi: 10.1073/pnas.1702041114.

Wu Z, Li M, Dong OX, Xia S, Liang W, Bao Y, Wasteneys G, Li X. 2019. Differential regulation of TNL-mediated immune signaling by redundant helper CNLs. *New Phytol* **222**:938-953. doi: 10.1111/nph.15665.

Wróblewski T, Spiridon L, Martin EC, Petrescu AJ, Cavanaugh K, Truco MJ, Xu H, Gozdowski D, Pawłowski K, Michelmore RW, Takken FLW. 2018. Genome-wide functional analyses of plant coiled–coil NLR-type pathogen receptors reveal essential roles of their N-terminal domain in oligomerization, networking, and immunity. *PLoS Biol* **16**:e2005821. doi: 10.1371/journal.pbio.2005821.

Zacharias DA, Violin JD, Newton AC, Tsien RY. 2002. Partitioning of lipid-modified monomeric GFPs into membrane microdomains of live cells. *Science* **296**:913-916. doi: 10.1126/science.1068539.

Zhang L, Chen S, Ruan J, Wu J, Tong AB, Yin Q, Li Y, David L, Lu A, Wang WL, Marks C, Ouyang Q, Zhang X, Mao Y, Wu H. 2015. Cryo-EM structure of the activated NAIP2-NLRC4 inflammasome reveals nucleated polymerization. *Science* **350**:404-409. doi: 10.1126/science.aac5789.

Zhou M, Li Y, Hu Q, Bai XC, Huang W, Yan C, Scheres SH, Shi Y. 2015. Atomic structure of the apoptosome: mechanism of cytochrome c- and dATP-mediated activation of Apaf-1. *Genes Dev* **29:**2349-2361. doi: 10.1101/gad.272278.115.

Figures and figure supplements

Figure 1. Transposon-based truncation mutagenesis reveals a short 29 amino-acid region sufficient for NRC4-mediated cell death. (**A**) Overview of the strategy for transposon-based C-terminal random truncation of NRC4 proteins. Hairpin Mu-STOP transposon and MuA proteins forming Mu transpososome were used for *in vitro* transposition into target plasmid. The truncation libraries (NRC4^{DV}::Mu-STOP) were transformed into *Agrobacterium* for transient expression in *N. benthamiana* leaves. The tube, petri dish and syringe are not drawn to scale. (**B**) NRC4$_{1\text{-}29}$::Mu-STOP triggers cell death in *N. benthamiana* leaves. In total, 65 truncated variants of NRC4^{DV} were expressed in *N. benthamiana* leaves, and the cell death activities are described as cell death induction (orange, HR+) and no visible response (blue, HR-).

Figure 1—figure supplement 1. Images of *N. benthamiana* leaves expressing truncated NRC4^{DV}::Mu-STOP variants. The images were taken 7 days after agroinfiltration. “DV”, “WT” and “TL” describe autoactive NRC4^{DV} mutant, wild-type NRC4 and the truncation library, respectively. Red characters indicate clones triggering HR in *N. benthamiana* leaves.

Figure 2. NRC4$_{1\text{-}29}$-YFP induces cell death in *Nicotiana benthamiana* independently of endogenous NRC4. (**A**) Schematic representation of wild-type NRC4-YFP (NRC4^{WT}-YFP) and the variants used for the *in planta* expression assays. The colour code is: red represents

NRC4 1 to 29 amino acid region. (**B**) $NRC4_{1-29}$-YFP triggers cell death in wild-type *N. benthamiana* leaves. $NRC4^{WT}$-YFP, $NRC4^{DV}$-YFP, $NRC4_{1-29}$-YFP and YFP were co-expressed with the gene silencing suppressor p19 and photographed at 7 days after agroinfiltration. (**C, D**) $NRC4_{1-29}$-YFP triggers cell death in *N. benthamiana* independently of endogenous NRC4. Leaves of two independent *N. benthamiana nrc4a/b* lines were used for agroinfiltration assays as described in B. (**E, F, G**) Anti-GFP immunoblots of $NRC4^{WT}$-YFP, $NRC4^{DV}$-YFP, $NRC4_{1-29}$-YFP and YFP expressed in *N. benthamiana* wild-type and *nrc4a/b* mutants. Total proteins were prepared from wild-type and *nrc4a/b N. benthamiana* leaves at 1 day after agroinfiltration. Given that the full-length NLRs accumulate at much lower levels than the shorter peptide, we showed different exposures as indicated by the black line. Red asterisks indicate expected band sizes.

Figure 2—figure supplement 1. Knocking out of *NRC4a* and *NRC4b* in *Nicotiana benthamiana* impairs Rpi-blb2-mediated HR cell death. (**A**) Schematic representation of sgRNA positions targeting *NRC4a* and *NRC4b*. The PAM motifs are marked in blue, and the sequences of sgRNAs are marked in red. (**B**) Genotyping results of selected T2 *nrc4a/b* plants. Sequences of the two sgRNA positions in *NRC4a* and *NRC4b* were confirmed by amplicon sequencing. "Percentage" represents the proportion of Illumina reads belonging to each sequence category. (**C**) *NRC4* knockout lines did not exhibit any growth defects when compared to wild type plants. Photographs of five weeks old wild type and *nrc4a/b* knock out *N. benthamiana* plants. (**D**) Schematic representation showing the genetic dependency of Rpi-blb2, Pto, and Rx on different NRCs according to previous finding with virus-induced gene silencing analysis (Wu et al., 2017). (**E**) Rpi-blb2-mediated HR cell death was compromised in the *NRC4* knockout lines. Rpi-blb2/AVRblb2, Pto/AvrPto and Rx/CP were transiently expressed in leaves of wild type and *nrc4a/b N. benthamiana* according to the method described previously in Wu et al. (2017). The pictures were taken at 7 days after agroinfiltration.

Figure 2—figure supplement 2. $NRC4_{1-29}$-YFP cell death is compromised by YFP A206K mutation. (**A**) Schematic representation of $NRC4^{DV}$-YFP, $NRC4_{1-29}$-YFP and the variants used for the *in planta* expression assays. Arrowheads show A206K mutation site in YFP. The red colour represents NRC4 1 to 29 amino acid region. (**B, C**) YFP A206K mutation reduces $NRC4_{1-29}$-YFP cell death in wild-type *N. benthamiana* leaves. $NRC4^{DV}$-YFP, $NRC4_{1-29}$-YFP, YFP and the A206K variants were co-expressed with p19 and photographed at 7 days after agroinfiltration. Cell death-related autofluorescence was detected with Odyssey Infrared Imager (800 nm channel, LI-COR) (**D**) Box plots showing cell death intensity scored as an HR index based on three independent experiments. Statistical differences among the samples were analysed with Tukey's HSD test ($P < 0.01$). (**E**) *In planta* accumulation of NRC proteins. For anti-GFP immunoblots of $NRC4^{DV}$-YFP, $NRC4_{1-29}$-YFP, YFP and the mutant proteins, total proteins were prepared from wild-type *N. benthamiana* leaves at 36 hours after agroinfiltration. Red asterisks indicate expected band sizes.

Figure 3. NRC4 carries N-terminal sequences that are conserved across distantly related CC-NLRs. (**A**) Schematic representation of the different NLR domains used in TRIBE-MCL and phylogenetic analyses. (**B**) Distribution of plant NLRs across N-terminal domain tribes. The colour codes are: orange for dicot NLRs and blue for monocot NLRs. (**C**) NLRs from the same N-terminal tribe are dispersed across NLR phylogeny. The phylogenetic tree was generated in MEGA7 by the neighbour-joining method using the NB-ARC domain sequences of 988 CC-

NLRs identified from *N. benthamiana*, tomato, sugar beet, Arabidopsis, rice and barley. Tribe 1 to Tribe 4 members are marked with different colours as indicated in each panel. Red arrow heads indicate bootstrap support > 0.7 and is shown for the relevant nodes. The scale bars indicate the evolutionary distance in amino acid substitution per site. The full phylogenetic tree can be found in Figure 3—figure supplement 2.

Figure 3—figure supplement 1. Phylogenetic analysis of NLR proteins from dicot and monocot plant species. NLR proteins were predicted by NLR-parser from *N. benthamiana* (NbS-), tomato (Solyc-), Arabidopsis (AT-), sugar beet (Bv-), rice (Os-) and barley (HORVU-) proteomes, and were used for the MAFFT multiple alignment and phylogenetic analyses. The phylogenetic tree was constructed with the NB-ARC domain sequences in MEGA7 by the neighbour-joining method. Each leaf is labelled with different colour ranges indicating plant species. Well-supported TIR-NLR clade and NRC-superclade members are marked in blue and orange, respectively. The bootstrap supports (> 0.7) are indicated as texts. The scale bar indicates the evolutionary distance in amino acid substitution per site.

Figure 3—figure supplement 2. Phylogenetic analysis of CC-NLR proteins from dicot and monocot plant species. The phylogenetic tree was constructed with the NB-ARC domain sequences of CC-NLRs as described in Figure supplement 12. Each leaf is labelled with different colour ranges indicating plant species. Well-supported NRC-superclade members are marked in orange. The bootstrap supports (> 0.7) are indicated as texts. The scale bar indicates the evolutionary distance in amino acid substitution per site.

Figure 4. The MADA motif is a conserved unit at the very N-terminus of NRC4 and ZAR1. (**A**) Schematic representation of a classical CC-NLR protein highlighting the position of the MADA motif. Consensus sequence pattern of the MADA motif identified by MEME along with an alignment of NRC4 and ZAR1. Red boxes refer to residues conserved over 45% in Tribe 2 NLRs. (**B**) A structure homology model of NRC4 based on ZAR1 resistosome illustrating the position of the MADA motif. Each of the modelled five monomers is illustrated in cartoon representation. The colour code is: red for the MADA motif. The grey box highlights the N-terminal α helices, which contain the MADA motif. (**C**) Distribution of the MADA motif in tomato (left) and Arabidopsis (right) proteomes following HMMER searches with the MADA motif HMM. The number of proteins in each HMM score bin is shown. NLR and non-NLR proteins are shown in orange and blue, respectively. The dashed line indicates the cut-off used to define the most robust MADA-CC-NLR. NLRs with scores <10.0 were classified as MADA-like NLRs (MADAL-NLRs).

Figure 4—figure supplement 1. CC-NLRs have conserved protein sequence patterns in the beginning of the N-terminal domains. Consensus sequence patterns in N-terminal domains were identified by MEME from 226 Tribe 1, 102 Tribe 2, 83 Tribe 3 and 59 Tribe 4 members. Motif logos describe the N-terminal consensus patterns from proteins in each tribe, as highlighted in orange, and EDVID motif patterns, as shown in black boxes.

Figure 4—figure supplement 2. N terminus of NRC4 possesses a consensus pattern coined MADA motif. (**A**) Consensus sequence of the MADA motif. The MADA motif logo was generated by MEME from 87 N-terminal domains of Tribe 2 members. (**B**) Graphical representation of the MADA HMM used to screen MADA-CC-NLR. The three most abundant

amino acids at each position in the motif are shown by frequency and labelled with their one-letter code.

Figure 5. The MADA motif is conserved in ~20% of CC-NLRs. (**A**) Schematic representation of a classical CC-NLR protein highlighting the regions used for HMMER searches (MADA-HMM) and for TRIBE-MCL. (**B**) Occurrence of MADA/MADAL-CC-NLRs in representative species of monocots and dicots. The frequency of MADA/MADAL-CC-NLRs for each plant species was calculated as a percentage of all predicted CC-NLR proteins. (**C**) Occurrence of MADA/MADAL-CC-NLRs in N-terminal domain tribes of CC-NLRs. (**D**) Position distribution of MADA/MADAL motif relative to the start codon position among the identified 103 MADA-CC-NLRs and 129 MADAL-CC-NLRs. The colour codes are: orange for MADA-CC-NLRs, blue for MADAL-CC-NLRs and grey for other NLRs.

Figure 5—figure supplement 1. Bar graph of MADA/MADAL-CC-NLRs according to HMM score. (**A**) HMM score bar graph for CC-NLR database (988 proteins). MADA/MADAL-CC-NLRs from HMMER analysis are shown in orange and blue, respectively. (**B**) HMM score bar graph with plant species information. MADA/MADAL-CC-NLRs from dicot and monocot plant species are shown in orange and blue, respectively. (**C**) HMM score bar graph with N-terminal domain tribe information. MADA/MADAL-CC-NLRs in tribe 1-4 from Tribe-MCL analysis are shown in blue, red, green and pink, respectively. MADA/MADAL-CC-NLRs from the other N-terminal domain tribes are shown in grey.

Figure 6. NRC-dependent sensors (NRC-S) do not have the MADA motif. (**A**) Distribution of NRCs (NRC-H) and NRC-dependent sensors (NRC-S) across N-terminal domain tribes of CC-NLRs. Individual NLR members of the NRC superclade were classified based on phylogenetic analysis as described in Figure 3—figure supplement 2. The colour codes are: orange for the NRCs (NRC-H), blue for the NRC-sensors (NRC-S) and grey for other NLRs. (**B**) NRC-dependent sensors (NRC-S) do not contain the MADA motif. The phylogenetic tree of the 988 CC-NLRs described in Figure 3C is shown in the left panel with the NRC superclade marked by the grey lines. The NRC superclade phylogenetic tree is shown on the right panel and highlights the well-supported subclades NRC-H and the expanded NRC-S. The NRC-S clade is divided into NLRs that lack an N-terminal extension domain (NTD) prior to their CC domain and those that carry an NTD. MADA-CC-NLRs are highlighted in red in both trees. Red arrowheads mark bootstrap supports > 0.7 in relevant nodes. The scale bars indicate the evolutionary distance in amino acid substitution per site. The full phylogenetic tree can be found in Figure 3—figure supplement 2. Schematic representation of domain architecture of the depicted classes of NLR protein is also shown similar to the other figures but with the ~600 amino acid NTD shown in yellow.

Figure 7. L9, V10 and L14 triple mutation impairs cell death activity of autoimmune NRC4^{DV}. (**A**) Schematic representation of NRC4 and the mutated sites in the MADA motif. Mutated sites and substituted residues are shown as red characters in the NRC4 sequence alignment. (**B**) Cell death observed in *N. benthamiana* after expression of NRC4 mutants. *N. benthamiana* leaf panels expressing NRC4^{WT}-6xHA, NRC4^{DV}-6xHA, NRC4$^{3A/DV}$-6xHA and NRC4$^{3E/DV}$-6xHA were photographed at 5 days after agroinfiltration. (**C**) Box plots showing cell death intensity scored as an HR index based on three independent experiments. Statistical differences among the samples were analysed with Tukey's honest significance

difference (HSD) test (P < 0.01). (**D**) *In planta* accumulation of the NRC4 variants. For anti-HA immunoblots of NRC4 and the mutant proteins, total proteins were prepared from *N. benthamiana* leaves at 1 day after agroinfiltration. Empty vector control is described as EV. Equal loading was checked with Reversible Protein Stain Kit (Thermo Fisher).

Figure 7—figure supplement 1. $NRC4_{1\text{-}29}$-YFP cell death is compromised by L9, V10 and L14 triple mutation. (**A**) Schematic representation of $NRC4_{1\text{-}29}$-YFP, $ZAR1_{1\text{-}144}$-YFP and the variants used for the *in planta* expression assays. Arrowheads show triple alanine mutation sites in $NRC4_{1\text{-}29}$ and $ZAR1_{1\text{-}144}$. The colour code is: red represents NRC4 1 to 29 amino acid region. (**B**) L9, V10 and L14 triple mutation impairs $NRC4_{1\text{-}29}$-YFP cell death. Wild-type *N. benthamiana* leaves were inoculated with *Agrobacterium* strain including pTRBO::YFP, pTRBO::$ZAR1_{1\text{-}144}$-YFP, pTRBO::$ZAR1_{1\text{-}144}^{F9A/L10A/L14A}$-YFP, pTRBO::$NRC4_{1\text{-}29}$-YFP or pTRBO::$NRC4_{1\text{-}29}^{L9A/V10A/L14A}$-YFP and photographed at 7 days after agroinfiltration. Cell death-related autofluorescence was detected with Odyssey Infrared Imager (800 nm channel, LI-COR) (**C**) Box plots showing cell death intensity scored as an HR index based on three independent experiments. Statistical differences among the samples were analysed with Tukey's HSD test (P < 0.01). (**D**) *In planta* accumulation of NRC proteins. For anti-GFP immunoblots of $NRC4_{1\text{-}29}$-YFP, $ZAR1_{1\text{-}144}$-YFP and the mutant proteins, total proteins were prepared from wild-type *N. benthamiana* leaves at 3 days after agroinfiltration. Red asterisks indicate expected band sizes.

Figure 8. L9E, L13E and L17E single mutations impair cell death activity of autoimmune $NRC4^{DV}$. (**A**) Schematic representation of NRC4 and the glutamic acid (E) mutant scan of the MADA motif. Mutated sites are shown as red characters in the NRC4 sequence. (**B**) Cell death observed in *N. benthamiana* after expression of NRC4 mutants. *N. benthamiana* leaf panels expressing $NRC4^{WT}$-6xHA, $NRC4^{DV}$-6xHA and the corresponding E mutants were photographed at 5 days after agroinfiltration. (**C**) Box plots showing cell death intensity scored as an HR index based on three independent experiments. Statistical differences among the samples were analysed with Tukey's HSD test (P < 0.01). (**D**) *In planta* accumulation of the NRC4 variants. Immunoblot analysis was done as described in Figure 7D.

Figure 8—figure supplement 1. Alanine mutants do not compromise HR cell death triggered by autoactive NRC4. (**A**) Schematic representation of NRC4 and the alanine (A) mutant scan of the MADA motif. Mutated sites are shown as red characters in the NRC4 sequence. (**B**) Cell death observed in *N. benthamiana* after expression of NRC4 mutants. *N. benthamiana* leaf panels expressing $NRC4^{WT}$-6xHA, $NRC4^{DV}$-6xHA and the corresponding A mutants were photographed at 5 days after agroinfiltration. (**C**) Box plots showing cell death intensity scored as an HR index based on three independent experiments. Statistical differences among the samples were analysed with Tukey's HSD test (P < 0.01). (**D**) *In planta* accumulation of the NRC4 variants. Immunoblot analysis was done as described in Figure 7D.

Figure 8—figure supplement 2. Mapping loss of function mutations on N-terminal α helices of NRC4. (**A**) Cartoon representation of N-terminal α helices of NRC4 resistosome (zoom in grey box of Figure 4B). (**B, C**) N-terminal α helices are rotated 90 degrees and mutated amino acids are shown as stick representation and labelled.

Figure 9. NRC4$_{1\text{-}29}$-YFP forms MADA- and YFP-dependent puncta. (**A**) Subcellular localization of NRC4$_{1\text{-}29}$-YFP and the mutant proteins in *N. benthamiana* epidermal cells. *N. benthamiana* leaves expressing YFP, YFP^{A206K}, NRC4$_{1\text{-}29}$-YFP, NRC4$_{1\text{-}29}$-YFP^{A206K} and NRC4$_{1\text{-}29}^{L9E}$-YFP were imaged 2 days after agroinfiltration. (**B**) Single plain image of NRC4$_{1\text{-}29}$-YFP puncta. White dotted line indicates the tonoplast in *N. benthamiana* epidermal cell. White arrowheads point to NRC4$_{1\text{-}29}$-YFP puncta. Scale bars are 20 µm. (**C**) Quantification of puncta formation. The number of high intensity puncta was counted using maximum intensity Z-projection images from 12 independent observation. Statistical differences among the samples were analysed with Tukey's HSD test ($P < 0.01$).

Figure 10. First 17 amino acids of NRC4 can be functionally replaced by the N-terminus of other MADA/MADAL-CC-NLRs. (**A**) Alignment of the N-terminal region of the MADA/MADAL-CC-NLRs. Key residues for cell death activity identified in Figure 8 are marked as red characters with asterisks in the sequence alignment. Each HMM score is indicated. (**B**) Schematic representation of NRC4 MADA motif chimeras with MADA, MADAL and non-MADA sequences from other CC-NLRs. The first 17 amino acid region of other MADA-CC-NLR (orange), MADAL-CC-NLR (purple) or non-MADA-CC-NLR (grey) was swapped into NRC4^{DV}, resulting in the NRC4 chimeras with MADA/MADAL/non-MADA sequences originated from other NLRs. (**C**) Cell death phenotypes induced by the NRC4 chimeras. NRC4^{WT}-6xHA, NRC4^{DV}-6xHA and the chimeras were expressed in *N. benthamiana* leaves. Photographs were taken at 5 days after agroinfiltration.

Figure 10—figure supplement 1. Quantification of cell death triggered by NRC4 MADA motif chimeras. (**A**) Box plots showing cell death intensity scored as an HR index based on three independent experiments. Statistical differences among the samples were analysed with Tukey's HSD test ($P < 0.01$). (**B**) *In planta* accumulation of the NRC4 variants. Immunoblot analysis was done as described in Figure 7D.

Figure 11. The chimeric protein ZAR1$_{1\text{-}17}$-NRC4 complements NRC4 function in Rpi-blb2-mediated resistance. (**A**) Schematic representation of NRC4 complementation assay for Rpi-blb2-mediated resistance. Wild-type and the variants of NRC4 were co-expressed with RFP-Rpiblb2 in wild-type or *nrc4a/b*_9.1.3 *N. benthamiana* leaves by agroinfiltration. The leaves were inoculated with droplets of zoospore suspension from *P. infestans* strain 88069 at 1 day after the agroinfiltration. The syringe and pipet are not drawn to scale. (**B**) Disease and resistance phenotypes on NRC4/Rpi-blb2-expressed leaves. Images were taken under UV light at 7 days post inoculation. The lesion size (bottom panel) was measured in Fiji (Fiji Is Just ImageJ). Experiments were repeated three times with totally 84 inoculation site each. The numbers on the photographs indicate the sum of spreading lesions/total inoculation sites from the three replicates. Statistical differences among the samples were analysed with Tukey's HSD test ($P < 0.01$).

Figure 12. Evolution of NLRs from singletons to networks. We propose that the N-terminal MADA motif/α1 helix has emerged early in the evolution of CC-NLRs and has remained constrained throughout time as singletons evolved from multifunctional proteins into specialized paired and networked NLR helpers. In contrast, the MADA motif/α1 helix has degenerated in sensor CC-NLRs as they rely on their NLR helper mates for executing the

immune response ("use-it-or-lose-it" model of evolution). In addition, some sensor NLRs, such as a large subset of NRC-S proteins, have acquired N-terminal domains (NTDs)—prior to their CC domains—that function in pathogen detection. Such NTDs would preclude a free N-terminal α1 helix, which would be incompatible with the current model of ZAR1 resistosome activation.

Supplementary files

Supplementary file 1. Primers used for generating NRC4 variants by Golden Gate cloning.

Supplementary file 2. The MADA-HMM for HMMER analysis. This MADA-HMM was used for searching MADA-CC-NLRs from CC-NLR database (Figure 3—source data 1).

Source data files

Figure 1—source data 1. Sequences of NRC4 truncation library. The Mu-STOP transposon insertion sites were confirmed by PCR amplicon sequencing with Mu-STOP seq Rv primer. The 65 truncate sequences of NRC4 are listed in this file.

Figure 3—source data 1. Amino acid sequences of full-length NLRs in the CC-NLR database. 988 NLR sequences used for HMMER analysis are listed.

Figure 3—source data 2. Amino acid sequences of N-terminal domains in the CC-NLR database. N-terminal domain sequences of 988 proteins used for Tribe-MCL analysis are listed.

Figure 3—source data 3. N-terminal domain tribes of CC-NLRs. Results of the Tribe-MCL analysis are included in this file.

Figure 3—figure supplement 1—source data 1. Amino acid sequences for CC/TIR-NLR phylogenetic tree. NB-ARC domain sequences used for phylogenetic analysis are shown with the IDs, *N. benthamiana* (NbS-), tomato (Solyc-), Arabidopsis (AT-), sugar beet (Bv-), rice (Os-) and barley (HORVU-).

Figure 3—figure supplement 1—source data 2. CC/TIR-NLR phylogenetic tree file. The phylogenetic tree was saved in newick file format.

Figure 3—figure supplement 2—source data 1. Amino acid sequences for CC-NLR phylogenetic tree. NB-ARC domain sequences used for phylogenetic analysis are shown with the IDs, *N. benthamiana* (NbS-), tomato (Solyc-), Arabidopsis (AT-), sugar beet (Bv-), rice (Os-) and barley (HORVU-).

Figure 3—figure supplement 2—source data 2. CC-NLR phylogenetic tree file. The phylogenetic tree was saved in newick file format.

Figure 4—source data 1. Amino acid sequences of the MADA motif. The sequences were extracted from MEME output against N-terminal domain tribe 2 and were used to build the MADA motif HMM.

Figure 4—source data 2. Output of the HMMER search using the MADA motif HMM against tomato and Arabidopsis proteomes. HMM scores are listed with the IDs, tomato (Solyc-) and Arabidopsis (AT-), and annotation information.

Figure 5—source data 1. Output of the HMMER search using the MADA motif HMM against the CC-NLR database. HMM scores of the predicted MADA motifs are listed by IDs, *N. benthamiana* (NbS-), tomato (Solyc-), Arabidopsis (AT-), sugar beet (Bv-), rice (Os-) and barley (HORVU-), with Tribe-MCL result, the start ('MADA_strat') and end ('MADA_end') positions of the MADA motifs in the CC-NLRs.

Figure 5—source data 2. List of the predicted Arabidopsis MADA-CC-NLRs. The IDs are listed with the HMM score.

Figure 6—source data 1. HMM scores of NRC-superclade proteins. HMM scores are listed by IDs, *N. benthamiana* (NbS-), tomato (Solyc-) and sugar beet (Bv-) with Tribe-MCL result, the start ('MADA_strat') position of the MADA motifs and NRC clade information ('NRC-H' and 'NRC-S').

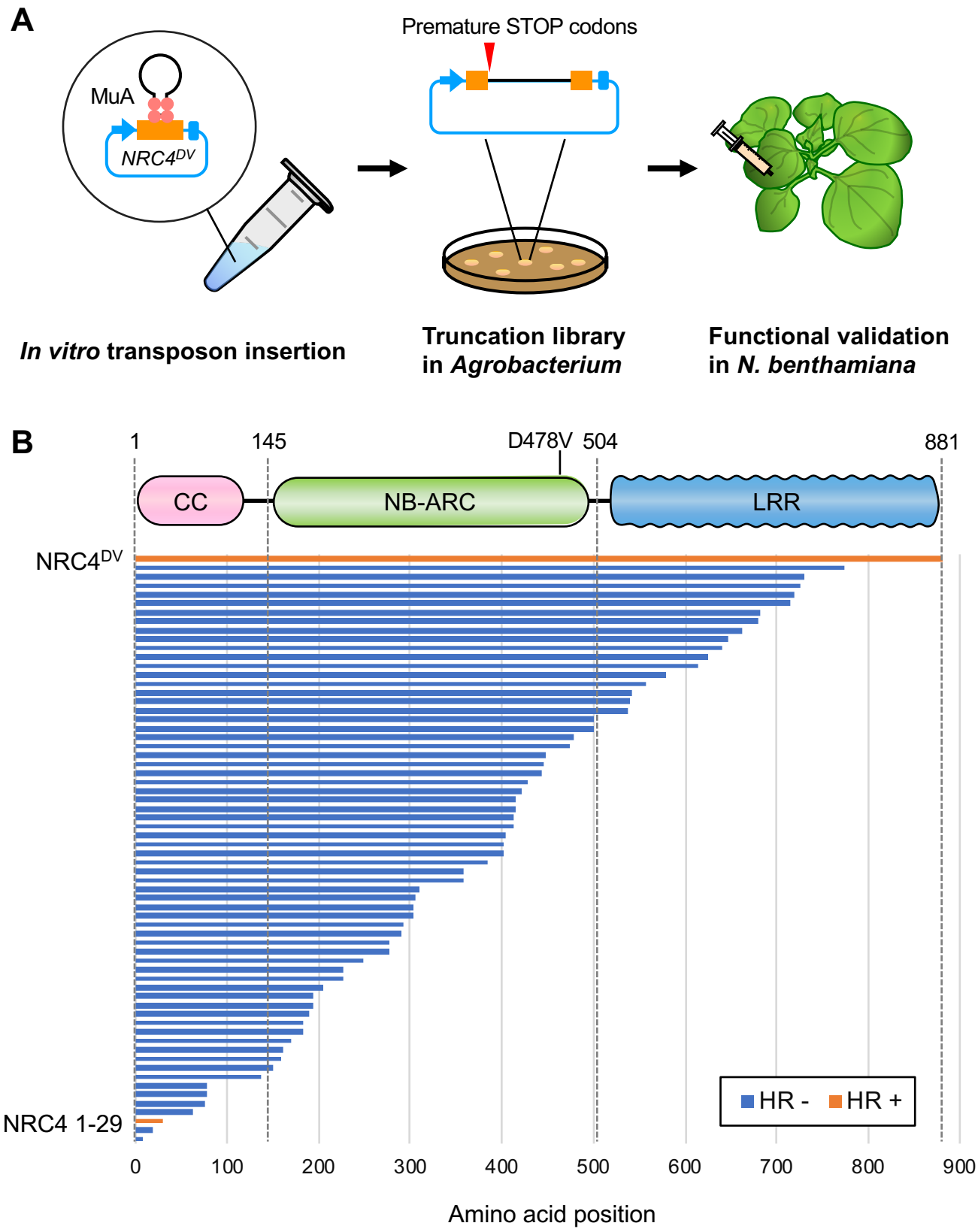

Figure 1. Transposon-based truncation mutagenesis reveals a short 29 amino-acid region sufficient for NRC4-mediated cell death.

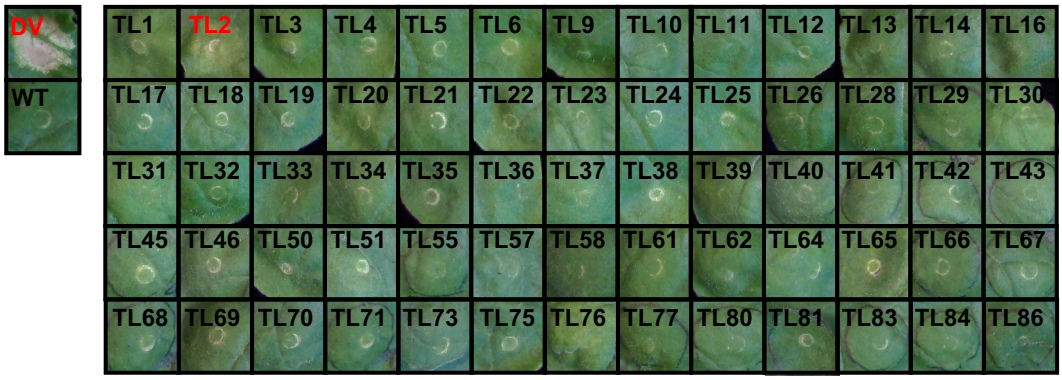

Figure 1—figure supplement 1. Images of *N. benthamiana* leaves expressing truncated NRC4^{DV}::Mu-STOP variants.

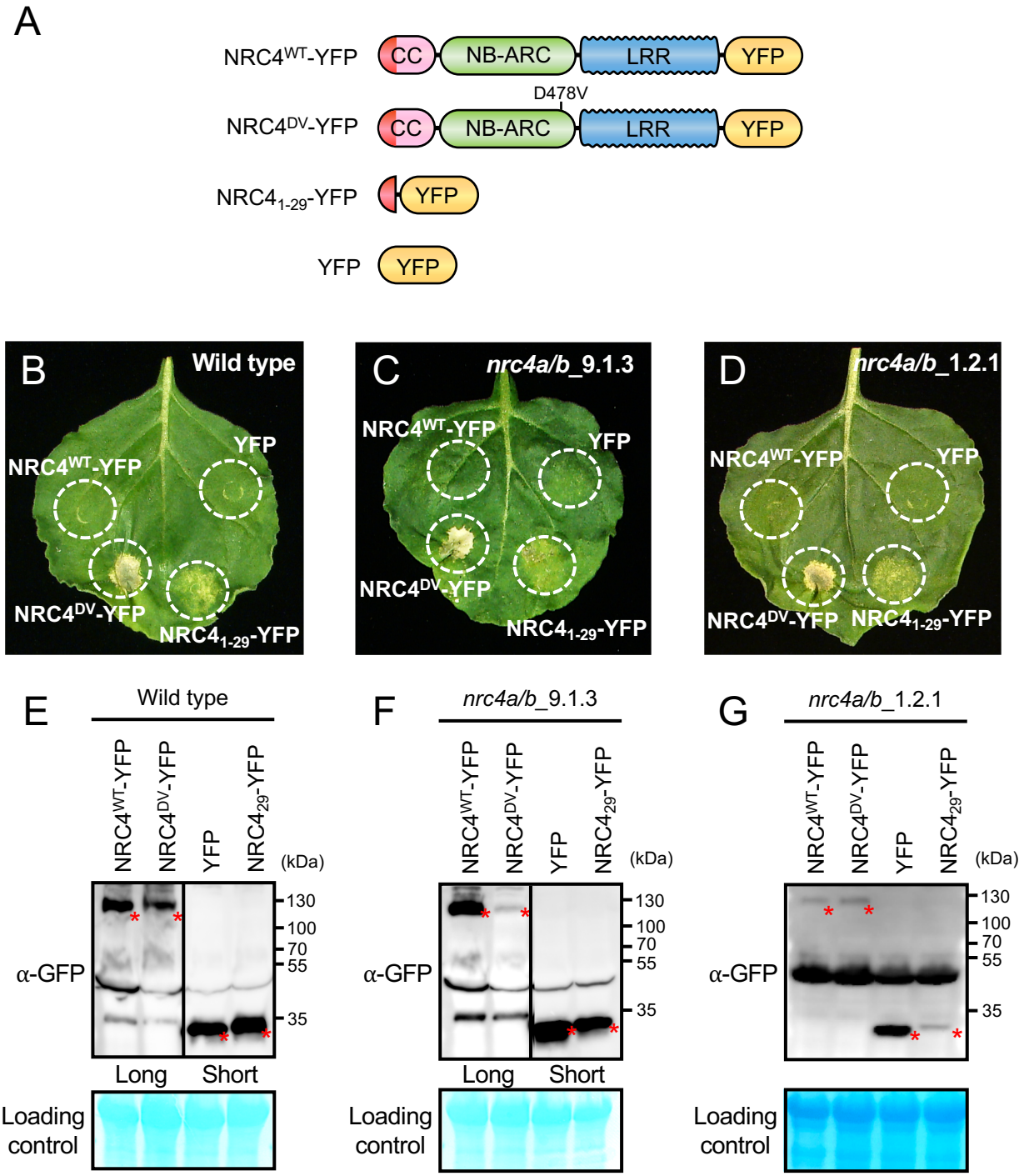

Figure 2. NRC4$_{1-29}$-YFP induces cell death in *Nicotiana benthamiana* independently of endogenous NRC4.

A

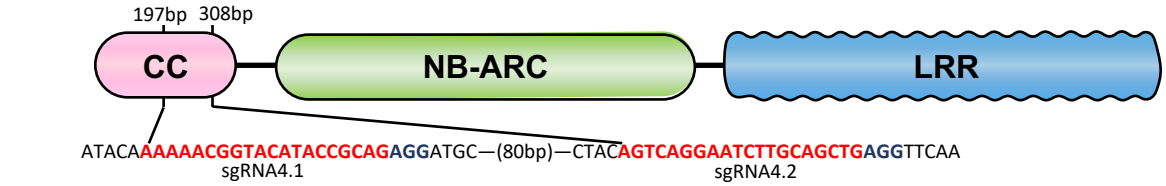

B

	Sequence (sgRNA4.1)	Sequence (sgRNA4.2)	Modification	percentage
WT	ATACAAAAAACGGTACATACCG--CAGAGGATGC—(80bp)—CTACAGTCAGGAATCTTGCAG--CTGAGGTTCAA		n/a	n/a
*nrc4a*_9.1.3	ATACAAAAAACGGTACATACCGACAGAGGATGC—(80bp)—CTACAGTCAGGAATCTTGCAG--CTGAGGTTCAA		1bp insertion, premature stop 77aa	44%
	ATACAAAAAA----------CG--CAGAGGATGC—(80bp)—CTACAGTCAGGAATCTTGCAG--CTGAGGTTCAA		10bp deletion, premature stop 119aa	54%
*nrc4b*_9.1.3	ATACAAAAAACGGTACATACC----CAGAGGATGC—(80bp)—CTACAGTCAGGAATCTTGCAG--CTGAGGTTCAA		1bp deletion, premature stop 123aa	99%
*nrc4a*_1.2.1	ATACAAAAAACGGTACATACCGACAGAGGATGC—(80bp)—CTACAGTCAGGAATCTTGCAG—CTGAGGTTCAA		1bp insertion, premature stop 77aa	56%
	ATACAAAAAACGGTACATACCGTCAGAGGATGC—(80bp)—CTACAGTCAGGAATCTT----------CTGAGGTTCAA		1bp insertion and 4 bp deletion premature stop 77aa	43%
*nrc4b*_1.2.1	ATACAAAAAACG----------CG--CAGAGGATGC—(80bp)—CTACAGTCAGGAATCTTGCAGACTGAGGTTCAA		9bp deletion and 1bp insertion premature stop 107aa	63%
	ATACAAAAAACG----------CG--CAGAGGATGC—(80bp)—CTACAGTCAGGAATCTTGCAG—CTGAGGTTCAA		9bp deletion, full length -3aa	20%
	ATACAAAAAACG----------CG--CAGAGGATGC—(80bp)—CTACAGTCAGGAATCTT----------CTGAGGTTCAA		9bp deletion and 4bp deletion premature stop 118aa	16%

C

D

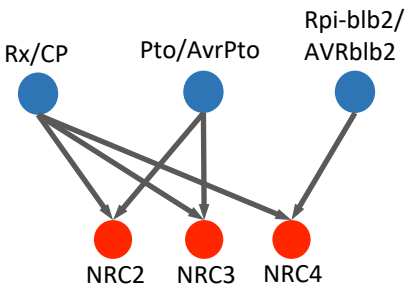

E

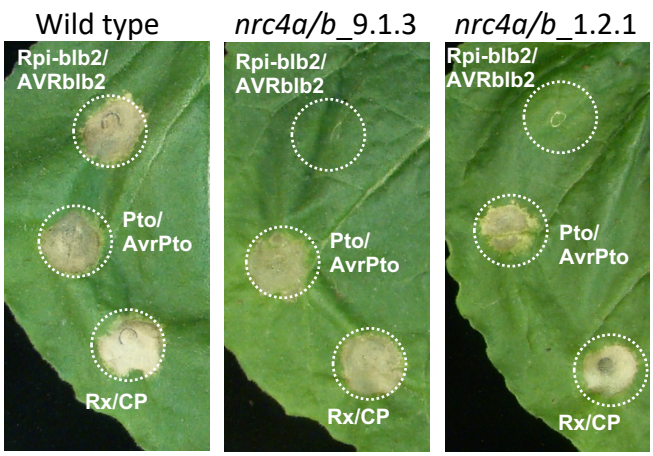

Figure 2—figure supplement 1. Knocking out of *NRC4a* and *NRC4b* in *Nicotiana benthamiana* impairs Rpi-blb2-mediated HR cell death.

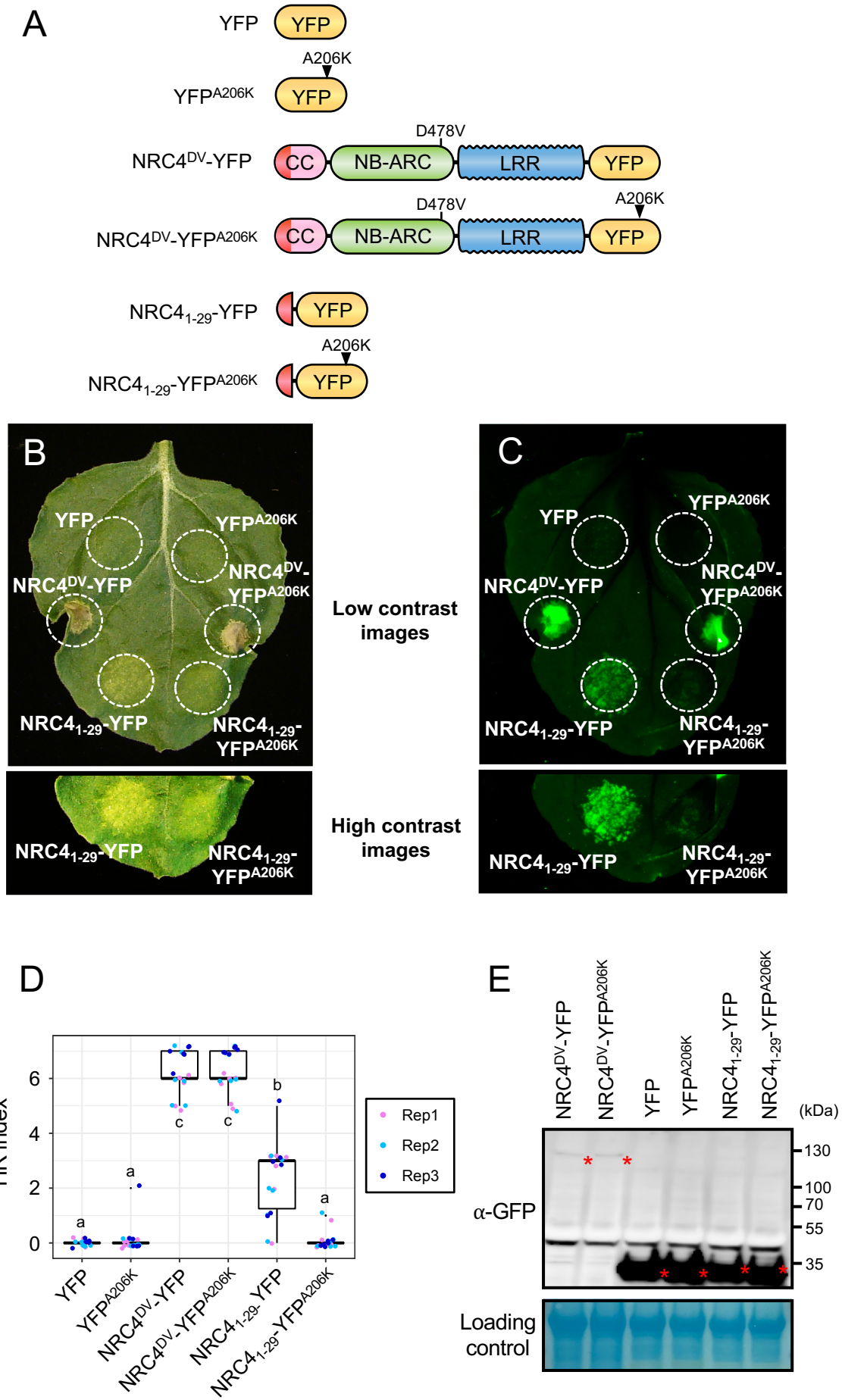

Figure 2—figure supplement 2. NRC4$_{1-29}$-YFP cell death is compromised by YFP A206K mutation.

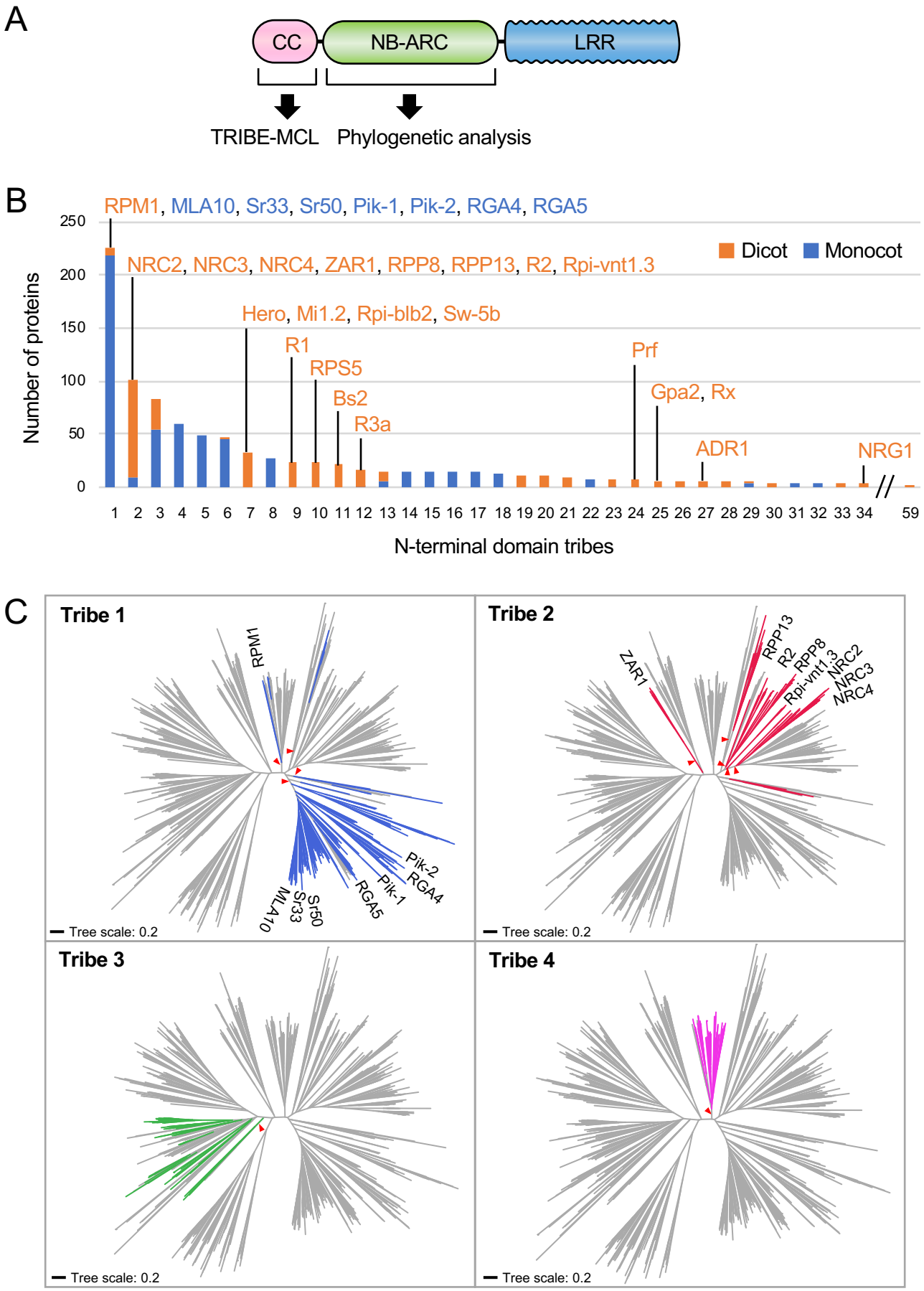

Figure 3. NRC4 carries N-terminal sequences that are conserved across distantly related CC-NLRs.

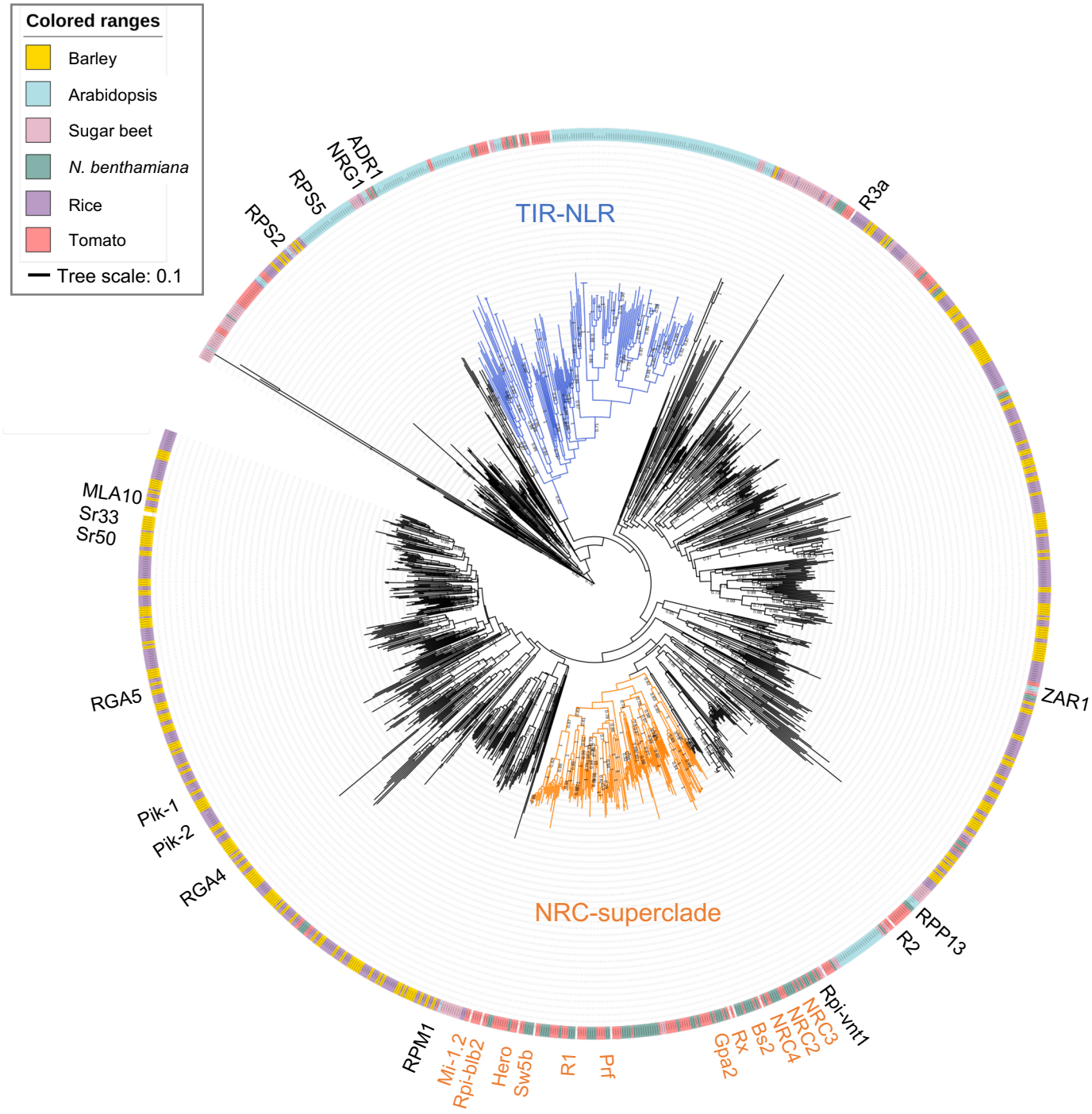

Figure 3—figure supplement 1. Phylogenetic analysis of NLR proteins from dicot and monocot plant species.

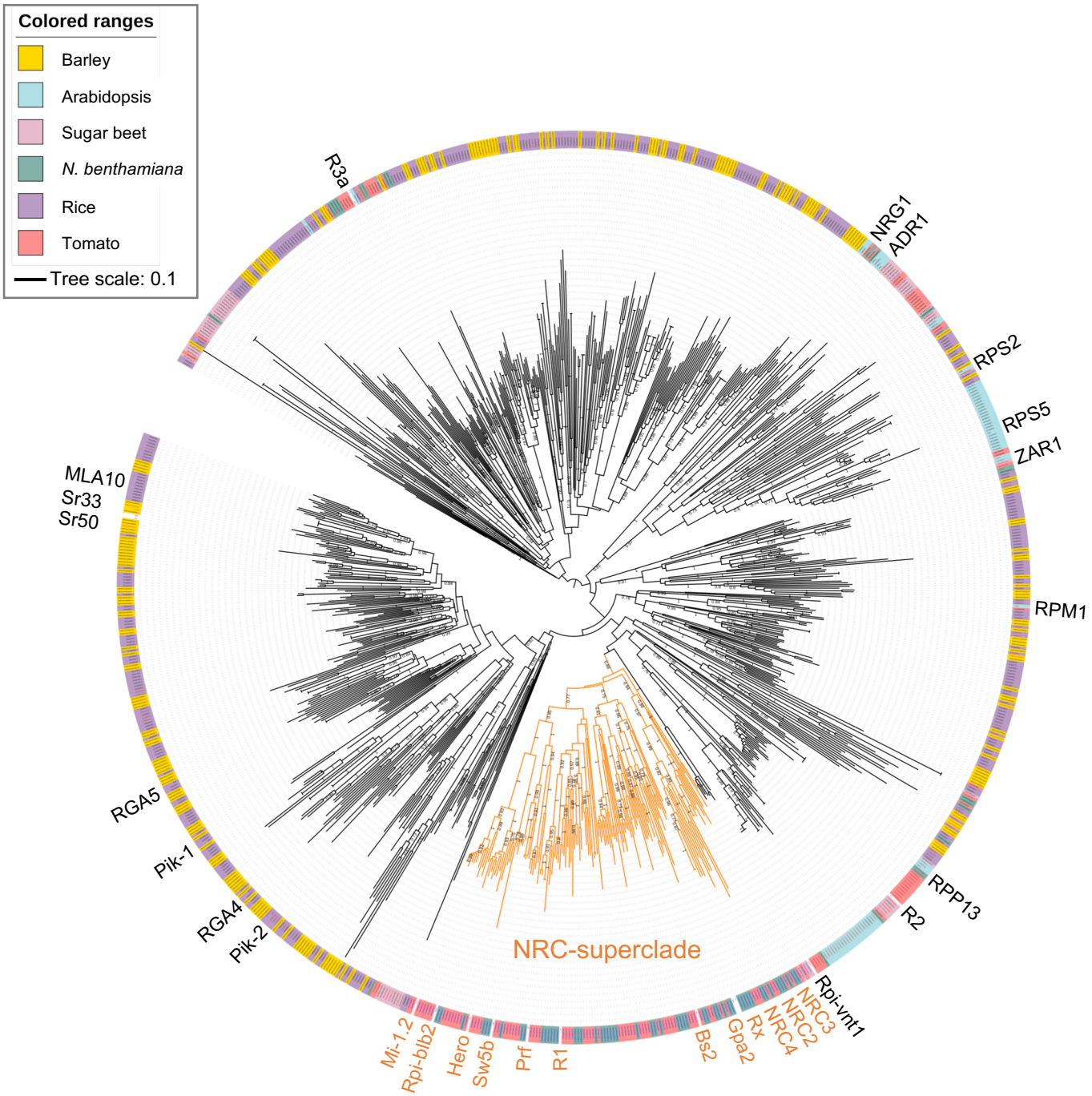

Figure 3—figure supplement 2. Phylogenetic analysis of CC-NLR proteins from dicot and monocot plant species.

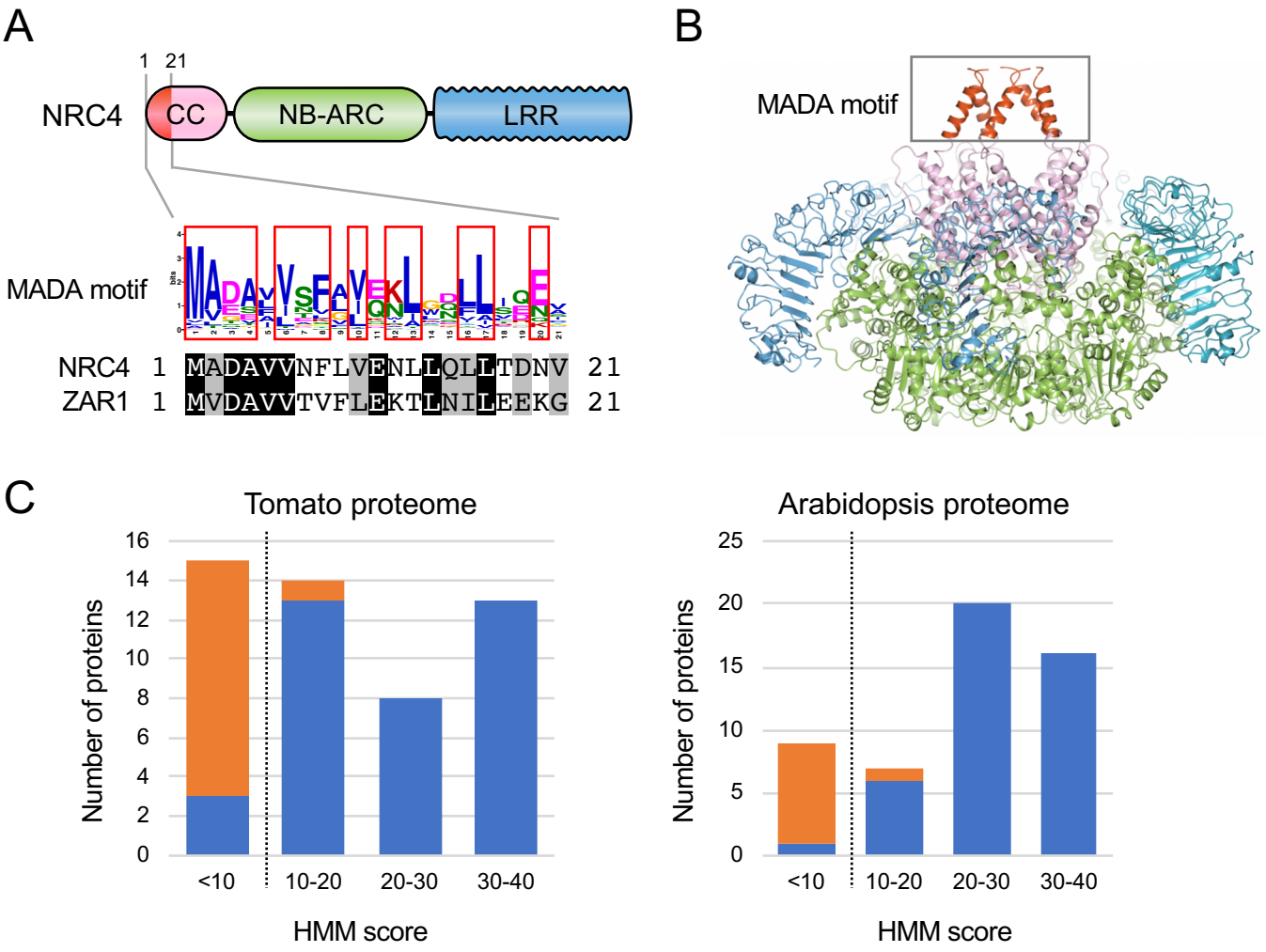

Figure 4. The MADA motif is a conserved unit at the very N-terminus of NRC4 and ZAR1.

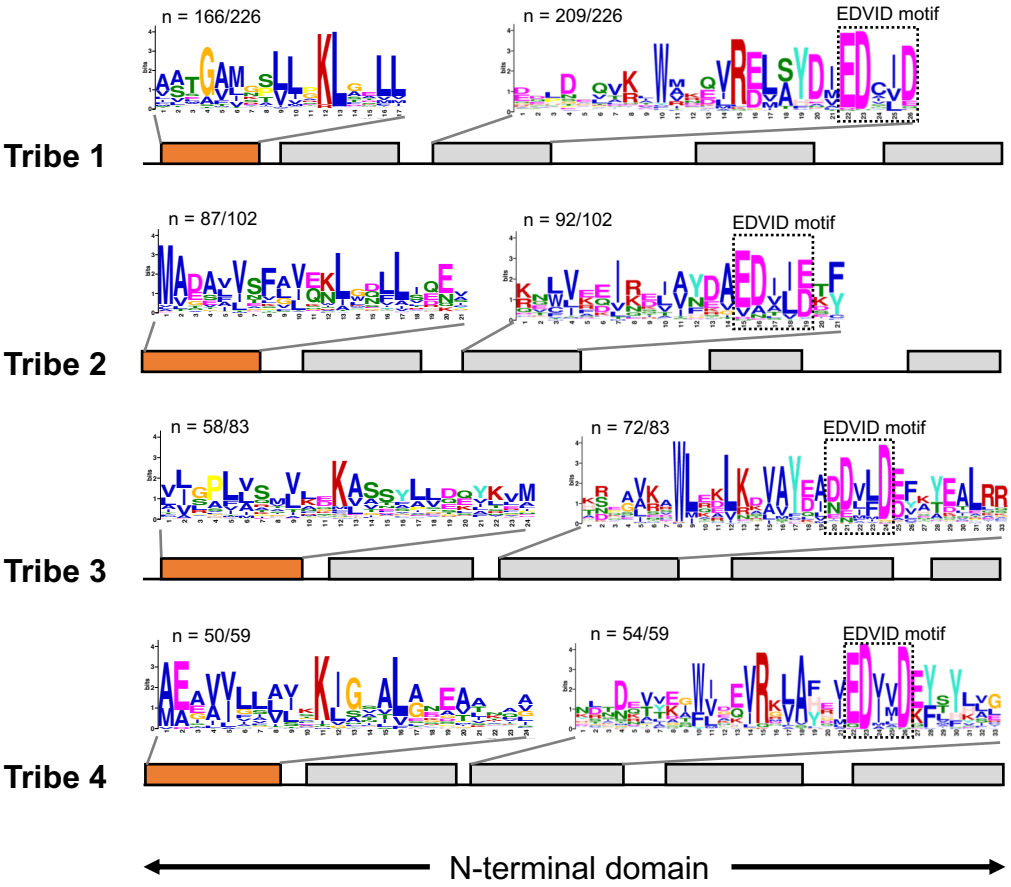

Figure 4—figure supplement 1. CC-NLRs have conserved protein sequence patterns in the beginning of the N-terminal domains.

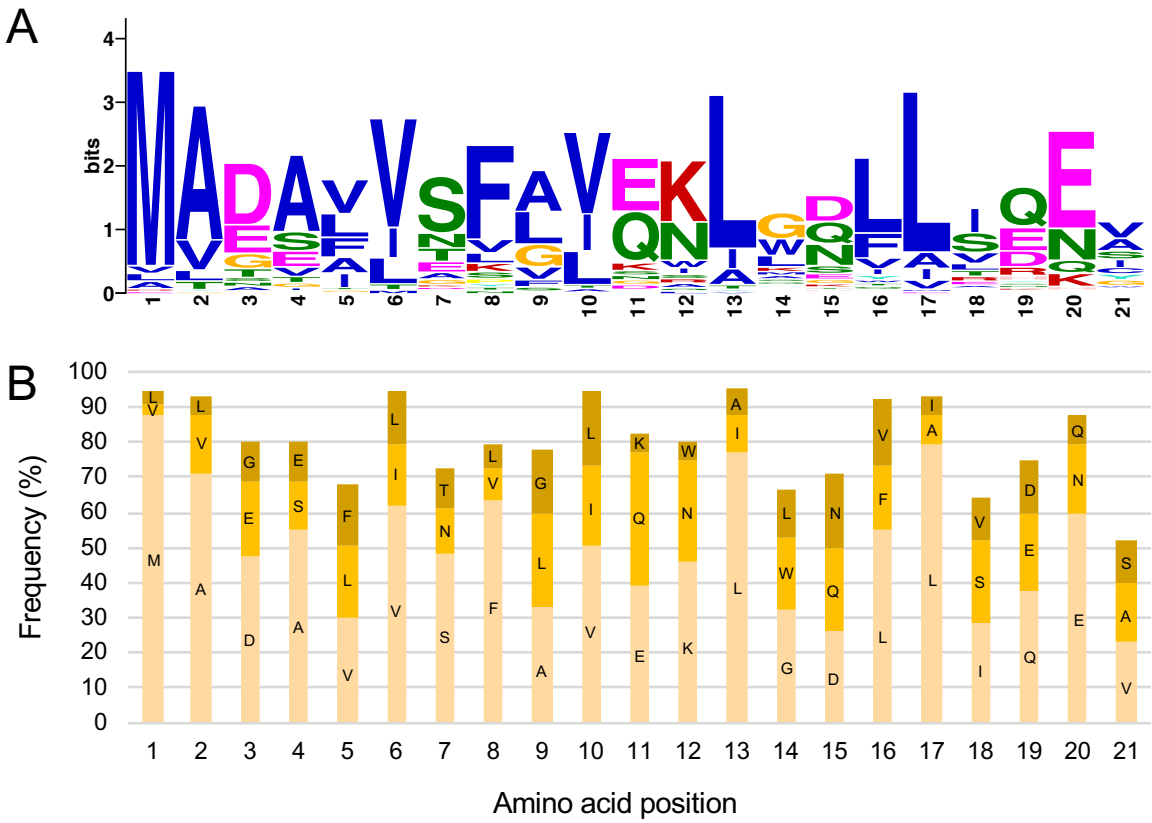

Figure 4—figure supplement 2. N terminus of NRC4 possesses a consensus pattern coined MADA motif.

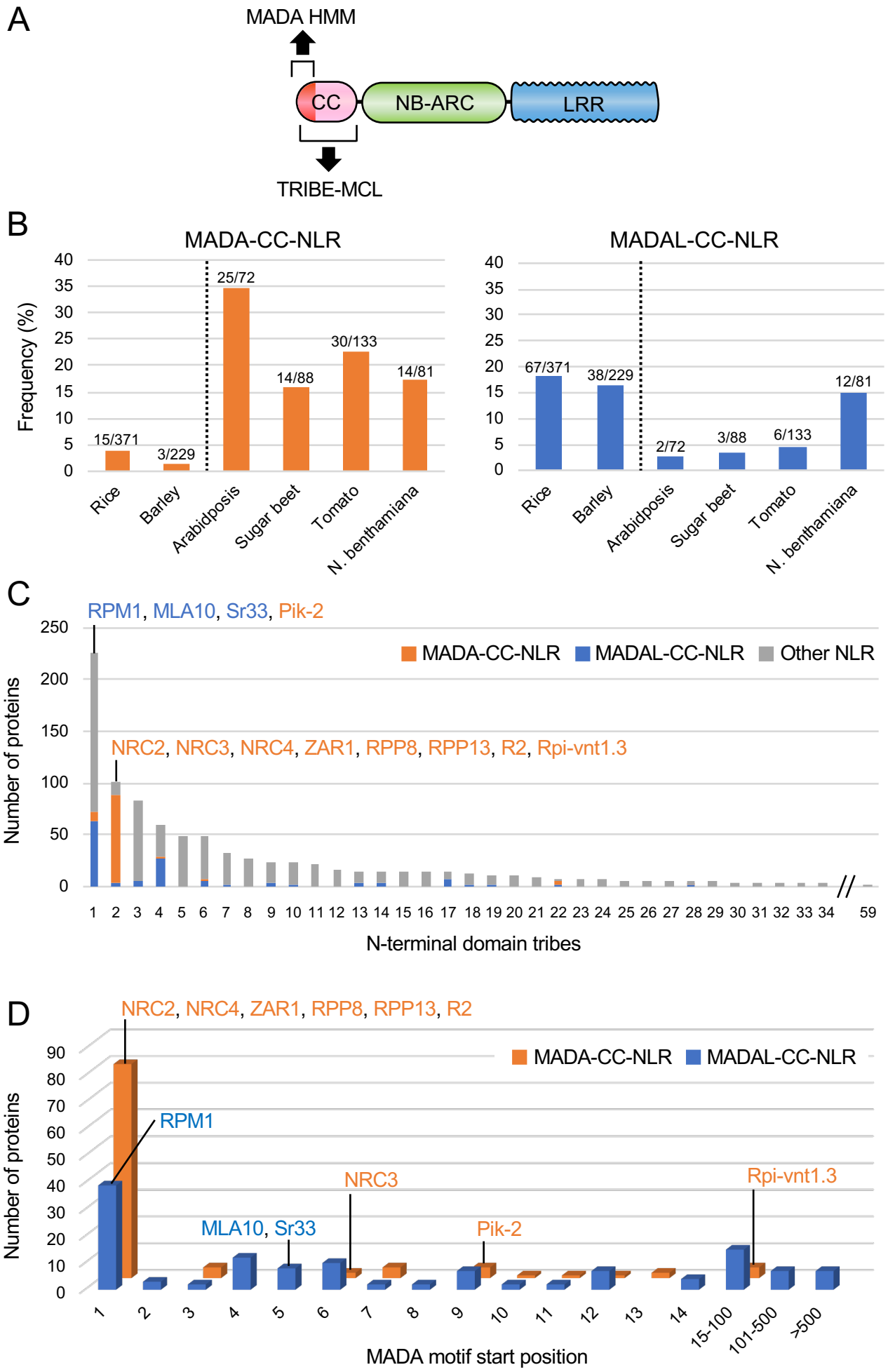

Figure 5. The MADA motif is conserved in ~20% of CC-NLRs.

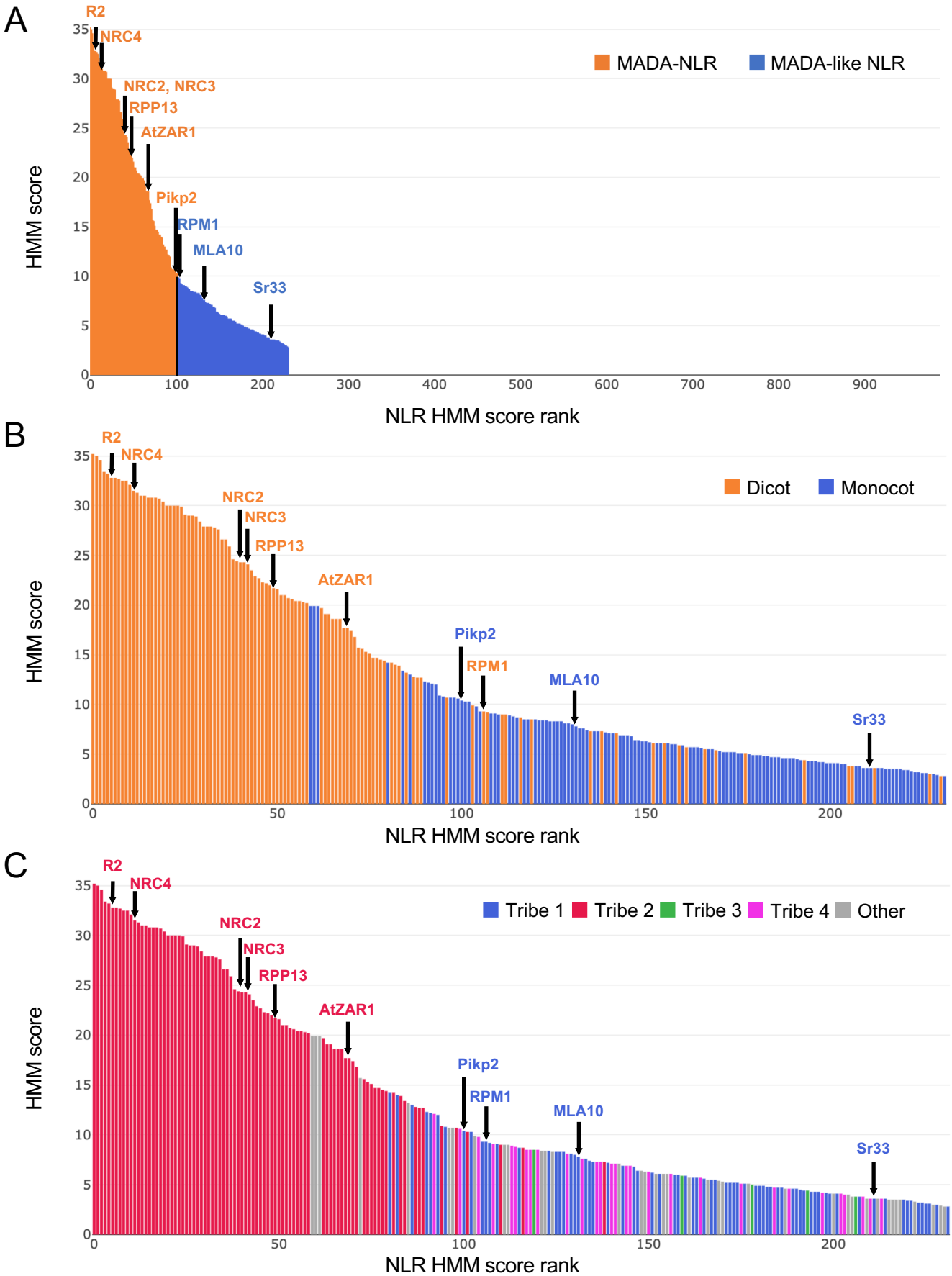

Figure 5—figure supplement 1. Bar graph of MADA/MADAL-CC-NLRs according to HMM score.

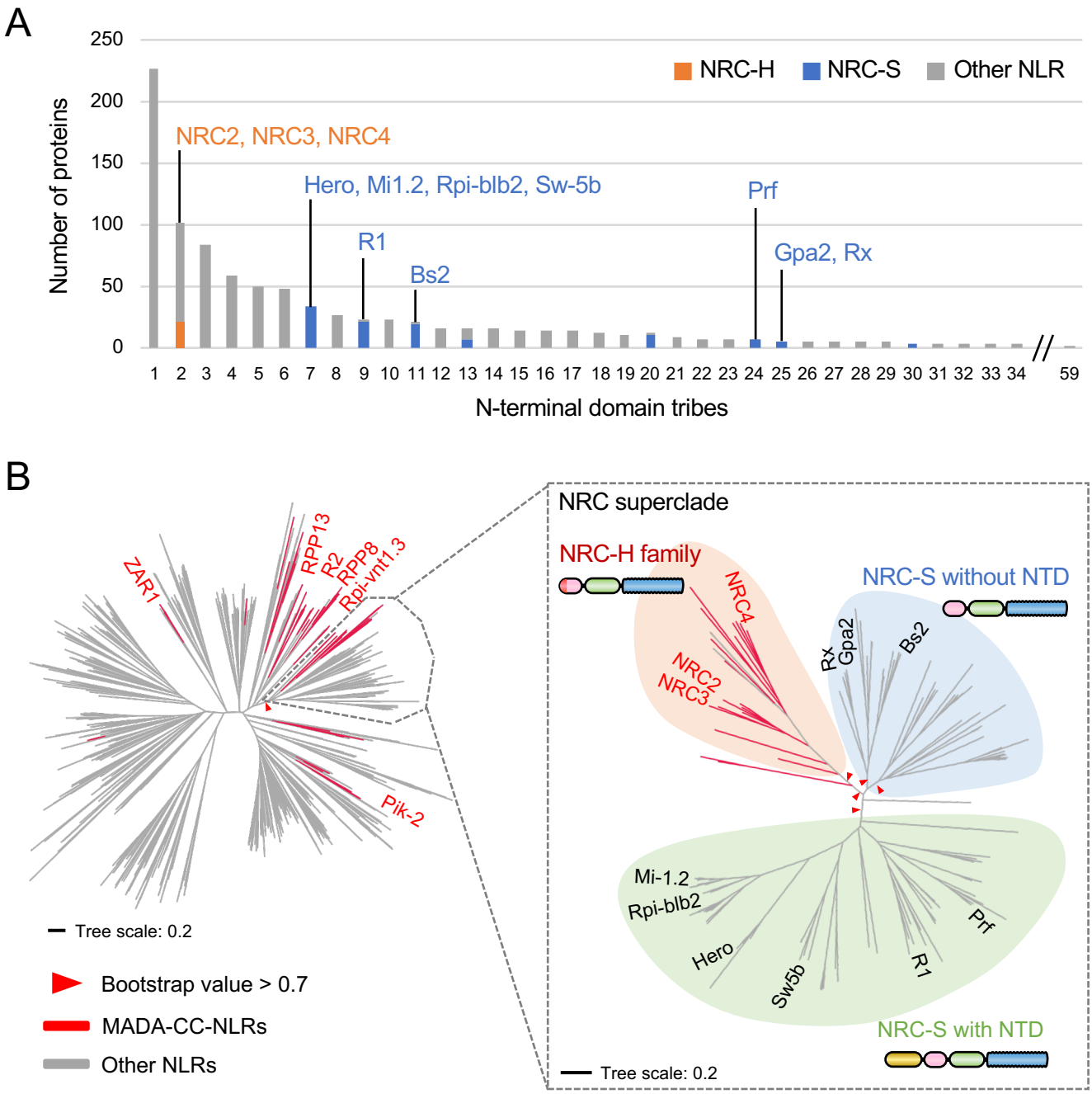

Figure 6. NRC-dependent sensors (NRC-S) do not have the MADA motif.

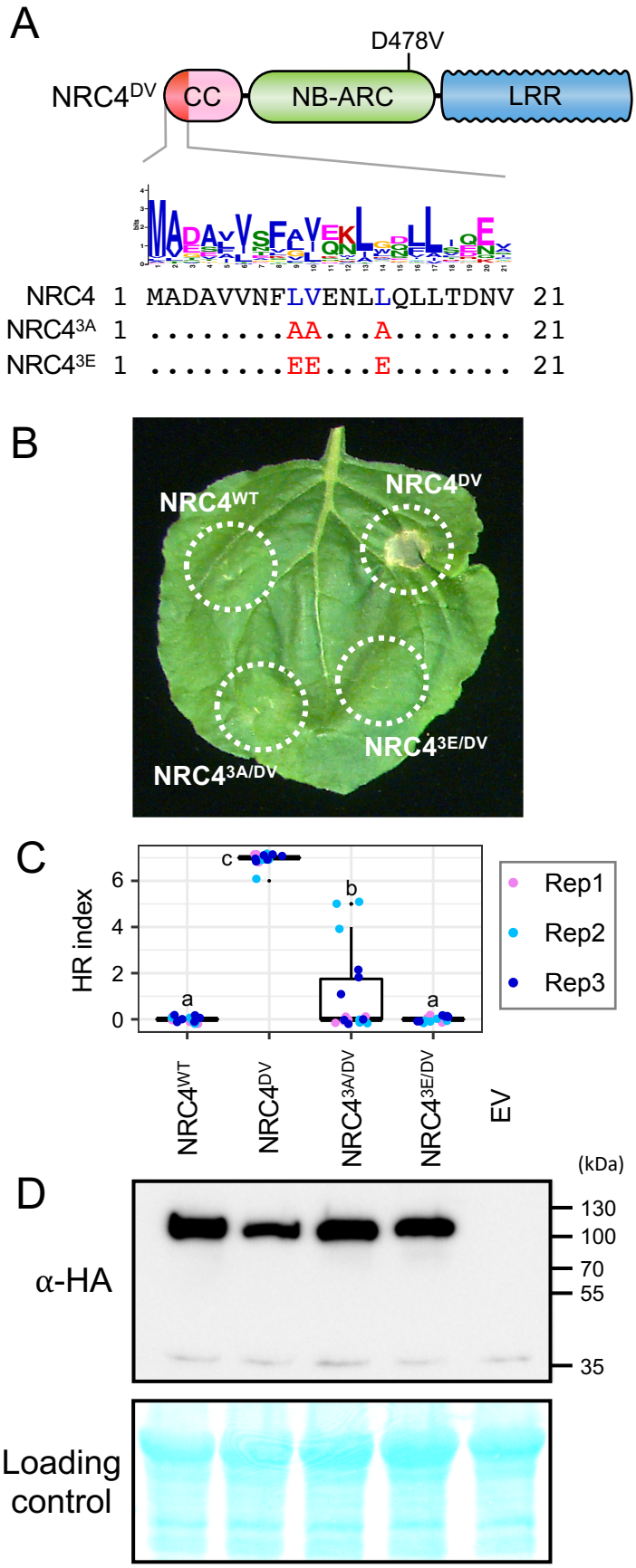

Figure 7. L9, V10 and L14 triple mutation impairs cell death activity of autoimmune NRC4^{DV}.

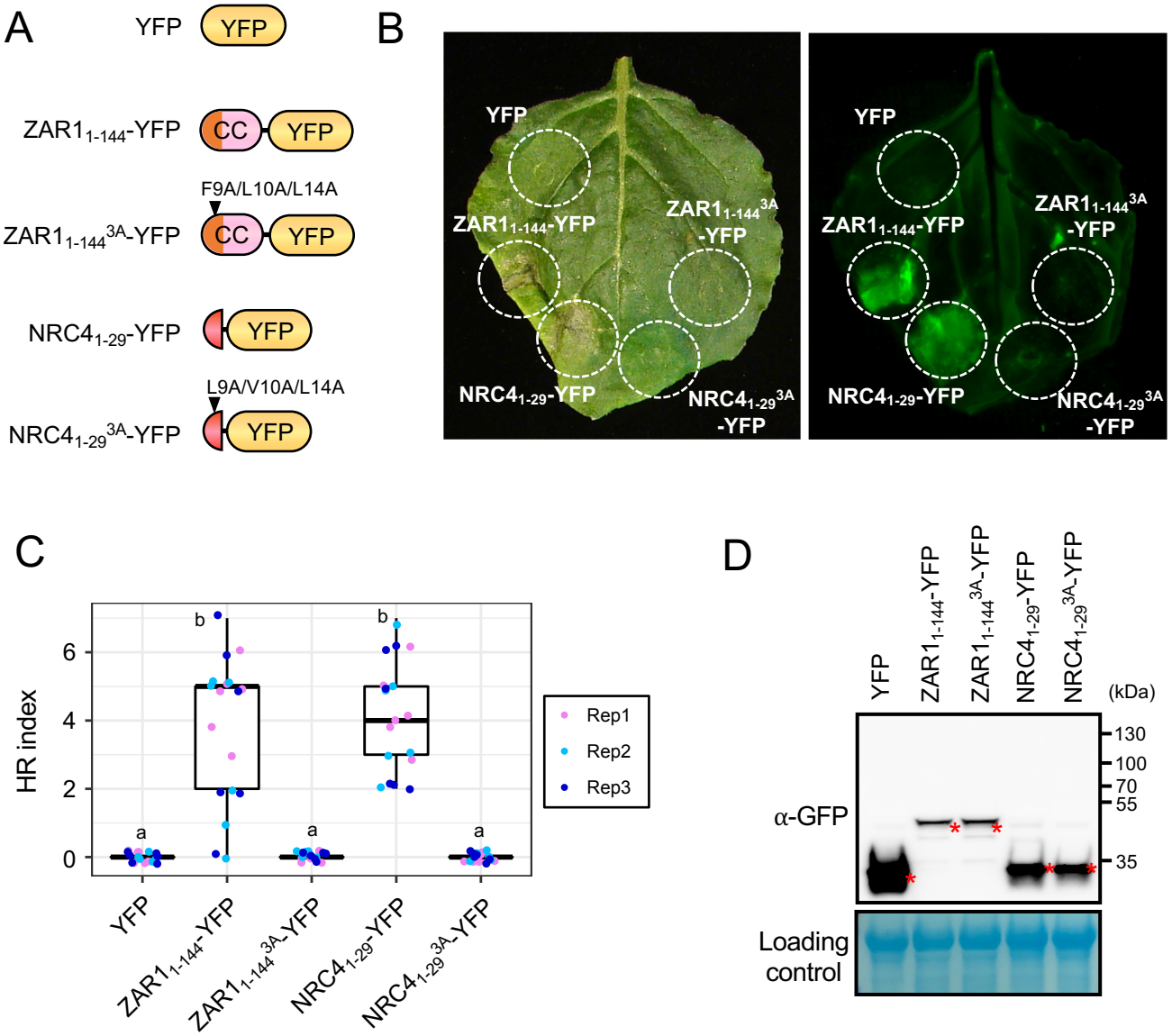

Figure 7—figure supplement 1. NRC4$_{1-29}$-YFP cell death is compromised by L9, V10 and L14 triple mutation.

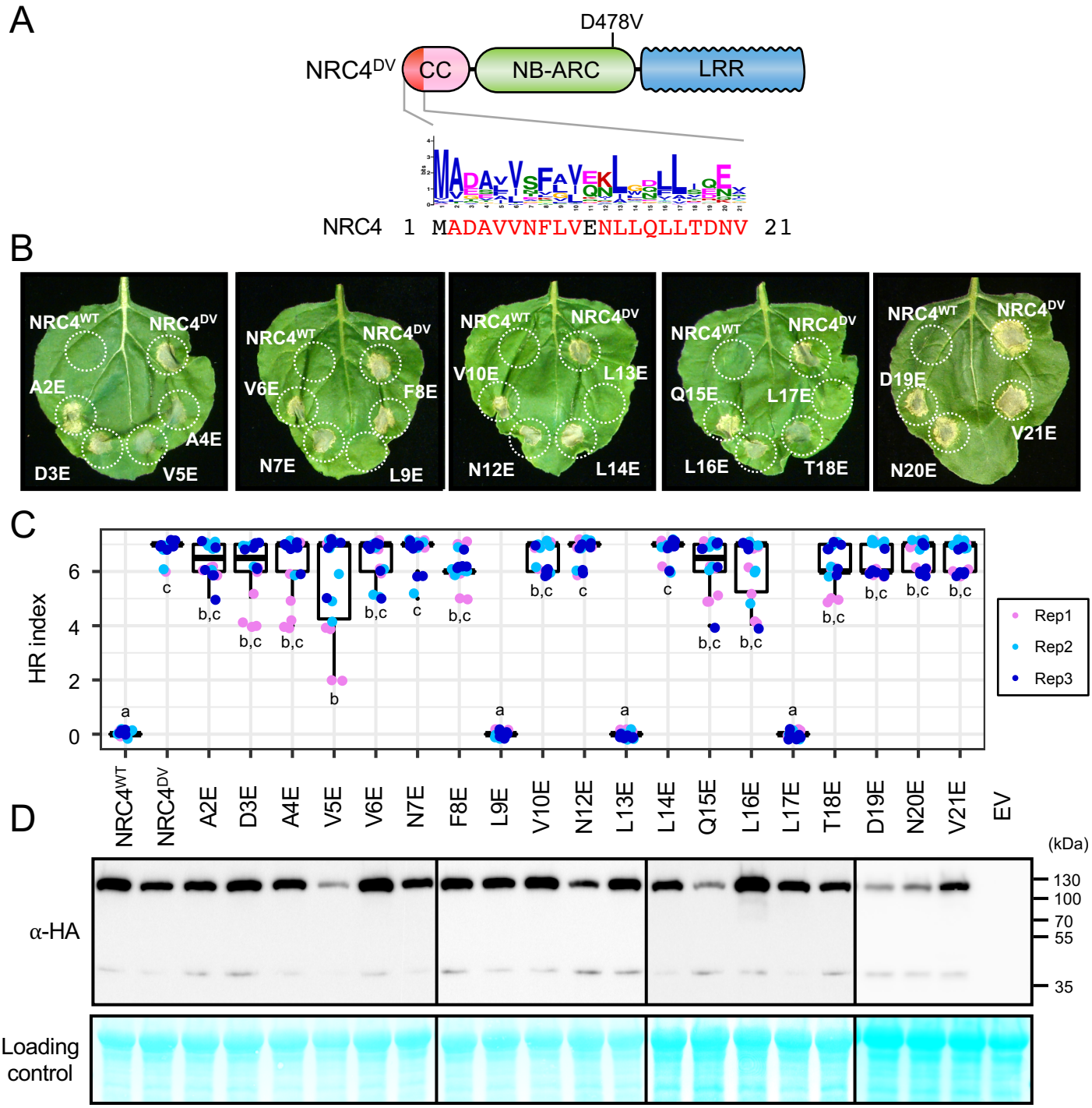

Figure 8. L9E, L13E and L17E single mutations impair cell death activity of autoimmune NRC4^{DV}.

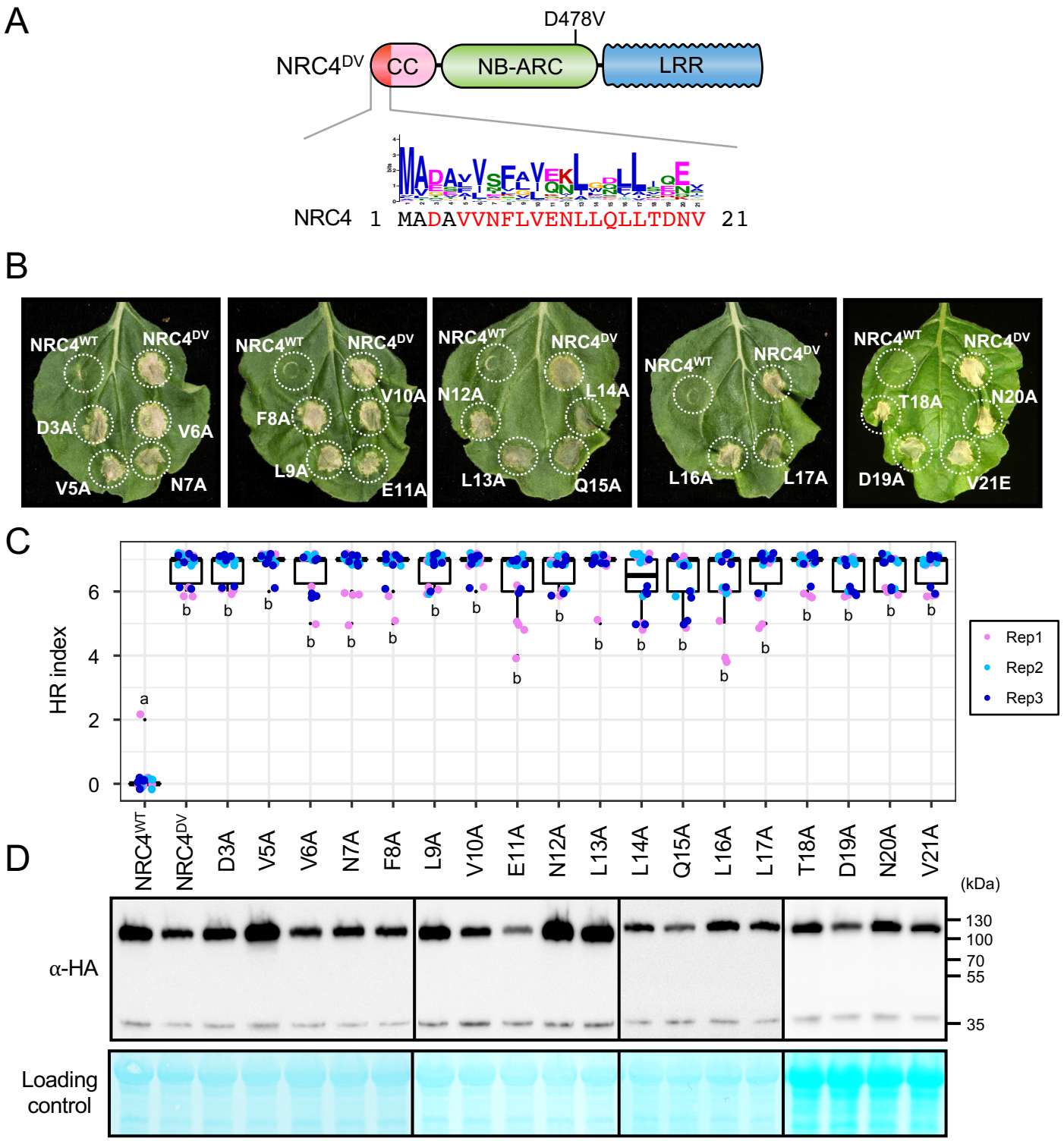

Figure 8—figure supplement 1. Alanine mutants do not compromise HR cell death triggered by autoactive NRC4.

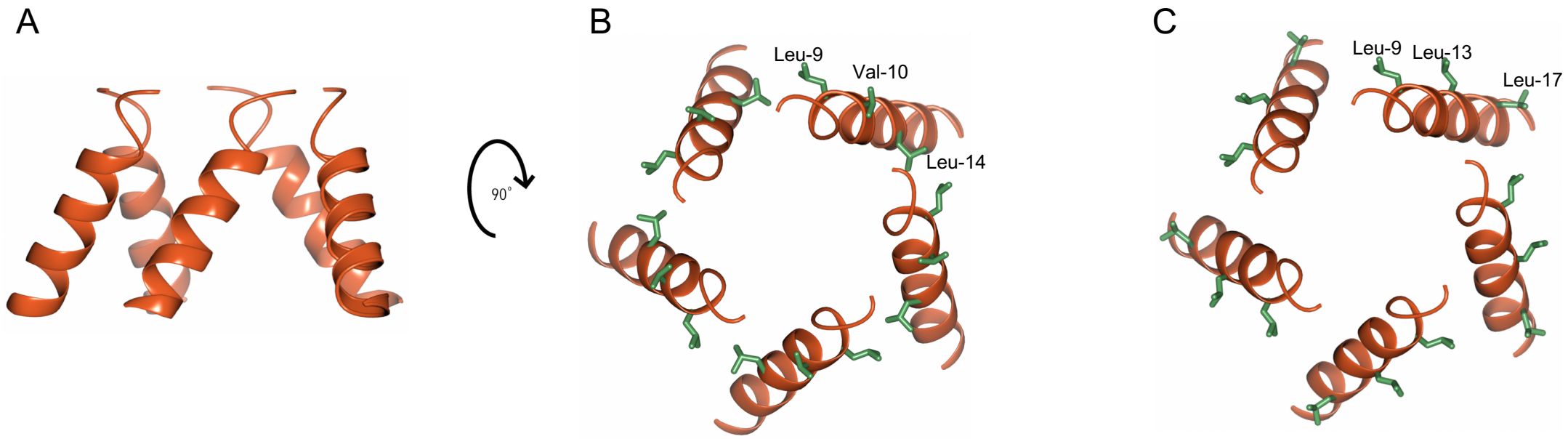

Figure 8—figure supplement 2. Mapping loss of function mutations on N-terminal a helices of NRC4.

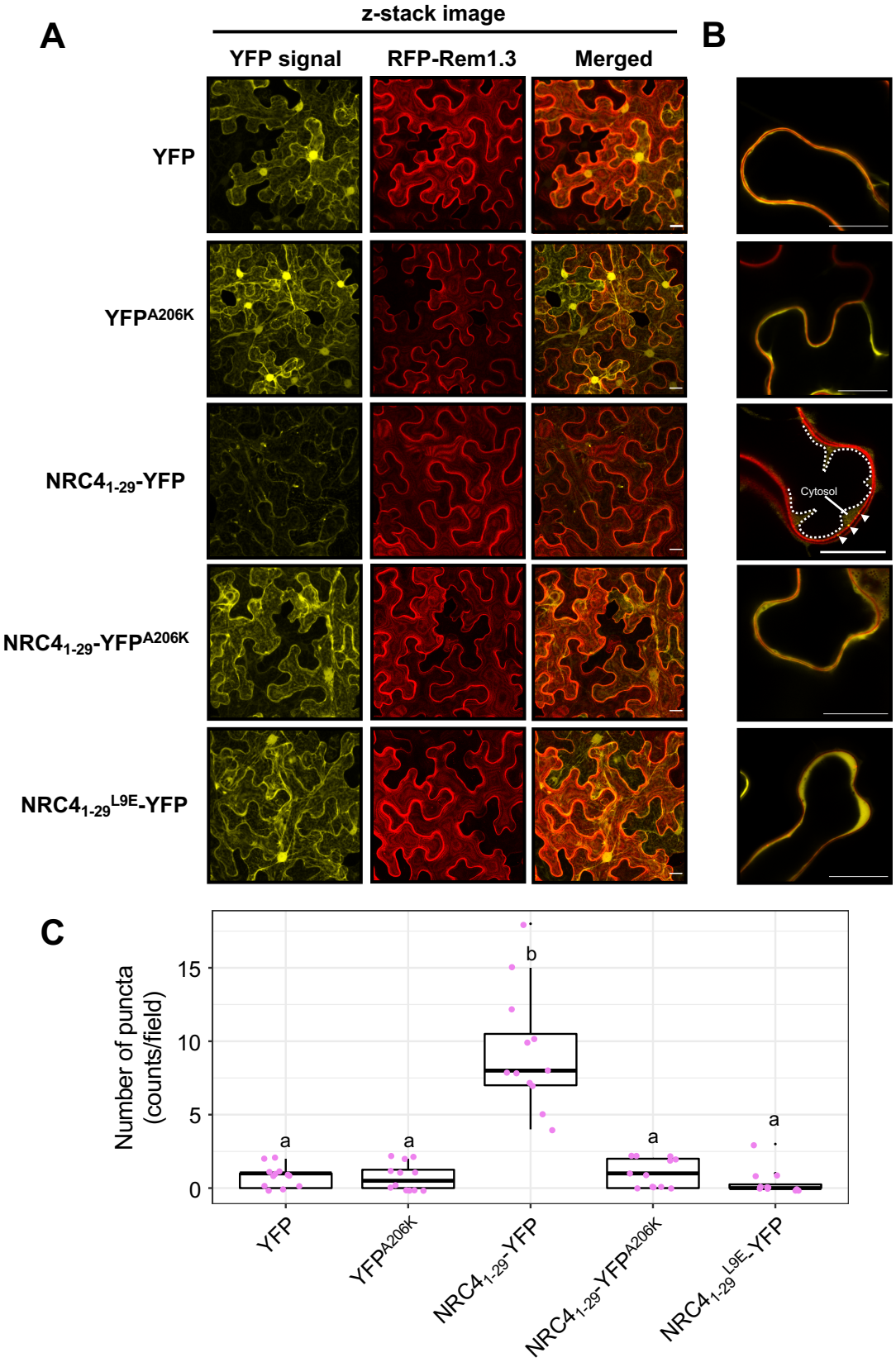

Figure 9. NRC4$_{1-29}$-YFP forms MADA- and YFP-dependent puncta.

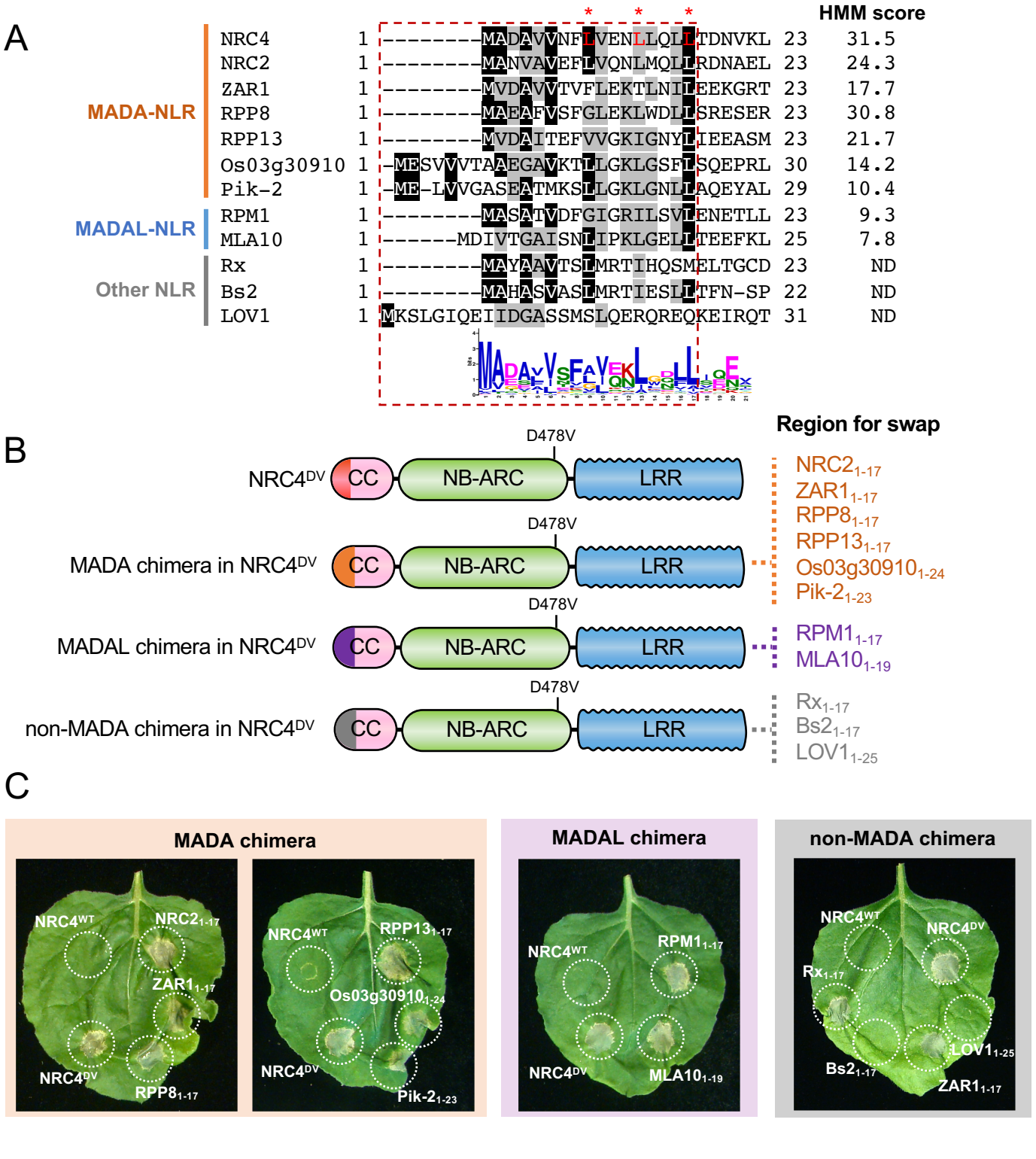

Figure 10. First 17 amino acids of NRC4 can be functionally replaced by the N-terminus of other MADA/MADAL-CC-NLRs.

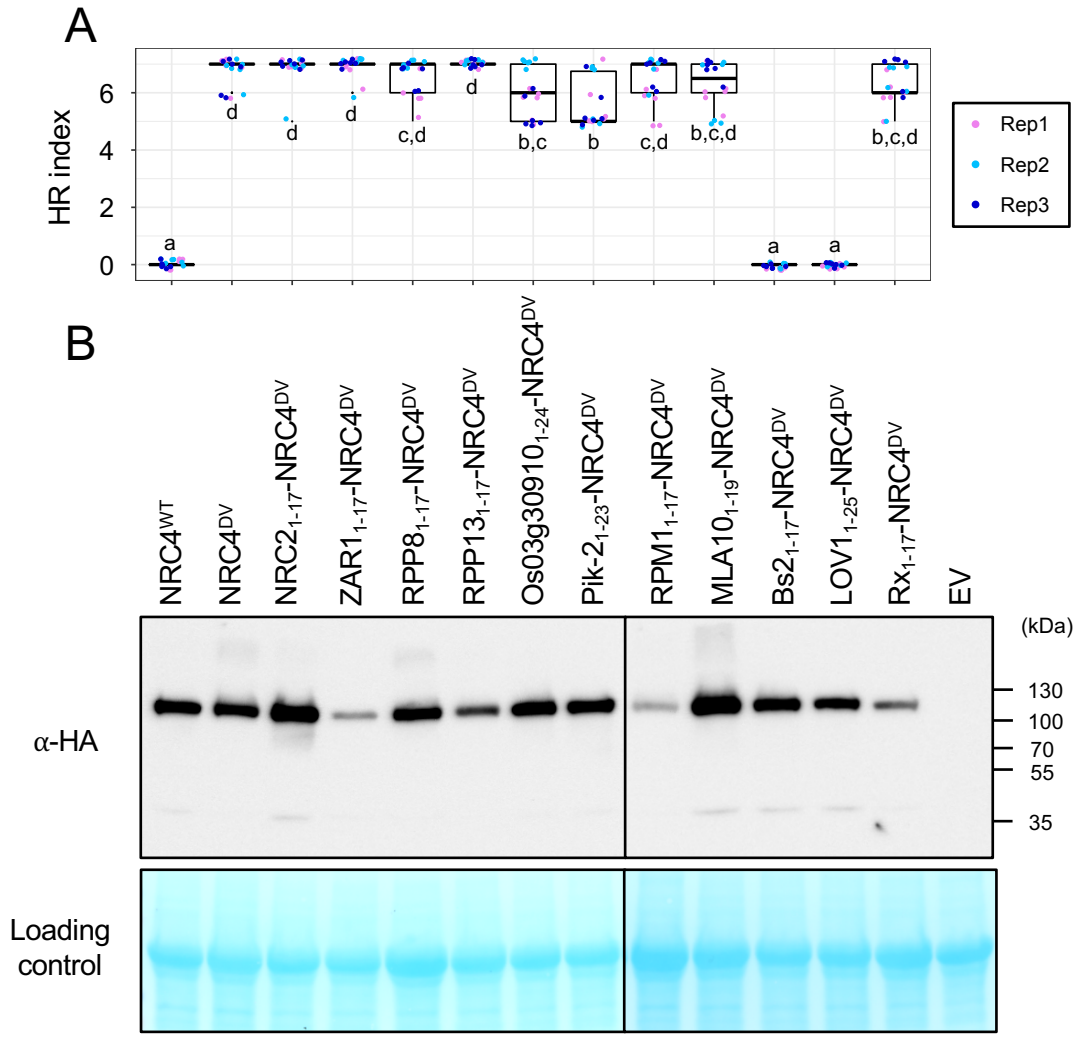

Figure 10—figure supplement 1. Quantification of cell death triggered by NRC4 MADA motif chimeras.

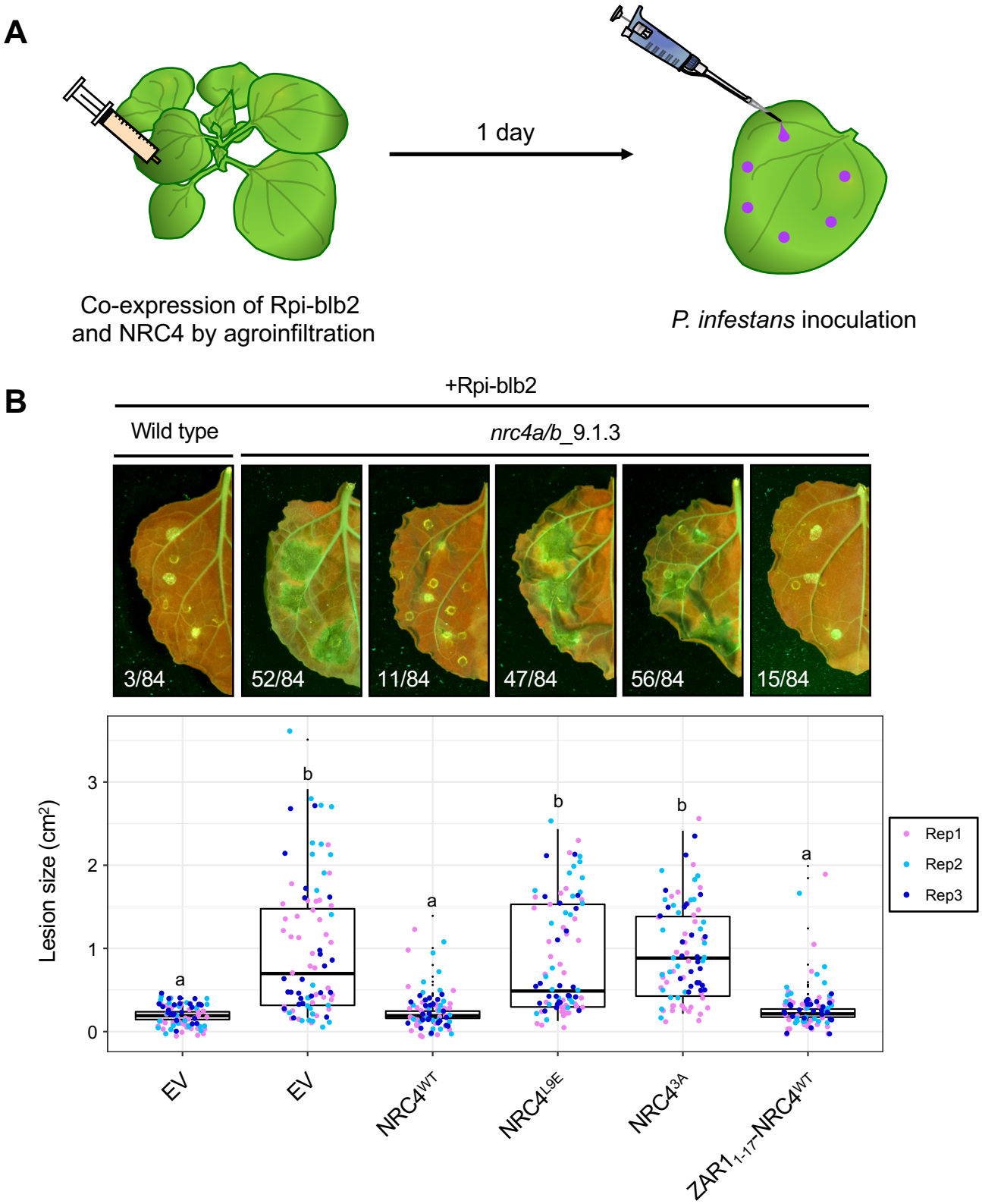

Figure 11. The chimeric protein ZAR1$_{1-17}$-NRC4 complements NRC4 function in Rpi-blb2-mediated resistance.

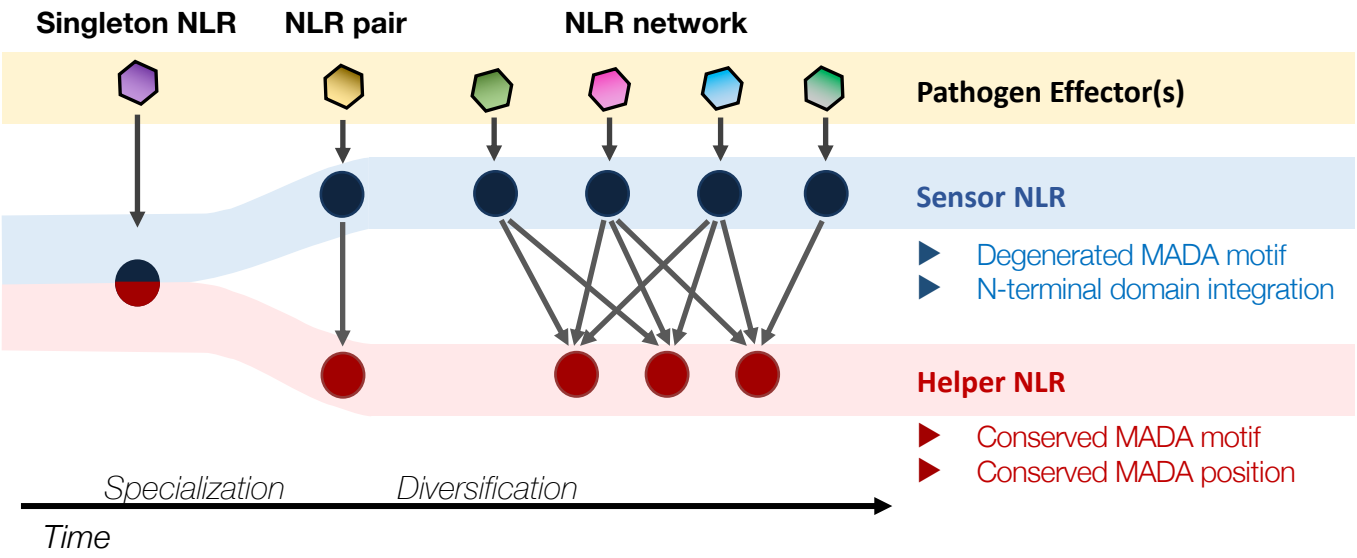

Figure 12. Evolution of NLRs from singletons to networks.